


ARTICLE

Atherogenic LOX-1 signaling is controlled by SPPL2-mediated intramembrane proteolysis

Torben Mentrup^{1,2}, Kosta Theodorou³, Florencia Cabrera-Cabrera^{1,2}, Andreas O. Helbig⁴, Kathrin Happ², Marion Gijbels^{3,5,6}, Ann-Christine Gradtk^{1,2}, Björn Rabe², Akio Fukumori⁷, Harald Steiner^{7,8}, Andreas Tholey⁴, Regina Fluhrer^{7,8}, Marjo Donners³, and Bernd Schröder^{1,2} 

The lectin-like oxidized LDL receptor 1 (LOX-1) is a key player in the development of atherosclerosis. LOX-1 promotes endothelial activation and dysfunction by mediating uptake of oxidized LDL and inducing pro-atherogenic signaling. However, little is known about modulators of LOX-1-mediated responses. Here, we show that the function of LOX-1 is controlled proteolytically. Ectodomain shedding by the metalloprotease ADAM10 and lysosomal degradation generate membrane-bound N-terminal fragments (NTFs), which we identified as novel substrates of the intramembrane proteases signal peptide peptidase-like 2a and b (SPPL2a/b). SPPL2a/b control cellular LOX-1 NTF levels which, following self-association via their transmembrane domain, can activate MAP kinases in a ligand-independent manner. This leads to an up-regulation of several pro-atherogenic and pro-fibrotic targets including ICAM-1 and the connective tissue growth factor CTGF. Consequently, SPPL2a/b-deficient mice, which accumulate LOX-1 NTFs, develop larger and more advanced atherosclerotic plaques than controls. This identifies intramembrane proteolysis by SPPL2a/b as a novel atheroprotective mechanism via negative regulation of LOX-1 signaling.

Introduction

Atherosclerosis and its clinical manifestations represent a leading cause of morbidity and mortality (Herrington et al., 2016). Vascular lesions called atherosclerotic plaques are hallmarks of the disease. Activation and dysfunction of endothelial cells and subendothelial accumulation of oxidized low-density lipoprotein (oxLDL; Steinberg et al., 1989; Di Pietro et al., 2016; Gimbrone and García-Cardeña, 2016) are initiating events for plaque formation (Gimbrone and García-Cardeña, 2016) by triggering immune cell recruitment. oxLDL activates endothelial cells via the lectin-like oxLDL receptor 1 (LOX-1; Sawamura et al., 1997). LOX-1 is a type II transmembrane protein that belongs to the family of C-type lectin receptors (Plato et al., 2013; Xu et al., 2013). The critical role of LOX-1 in atherosclerosis is well documented by in vivo studies in mice. Constitutive deletion or endothelial overexpression of LOX-1 attenuated or exacerbated the development of atherosclerotic plaques (Mehta et al., 2007; White et al., 2011; Akhmedov et al., 2014), establishing a pro-atherogenic function of this protein. This is supported by a

significant up-regulation of LOX-1 in human atherosclerotic lesions (Kataoka et al., 1999).

In addition to oxLDL uptake, LOX-1 triggers signaling pathways including the activation of mitogen-activated protein (MAP) kinases (Li and Mehta, 2000) and the NFκB pathway (Cominacini et al., 2000; Matsunaga et al., 2003). By this means, LOX-1 induces expression of adhesion molecules and pro-inflammatory cytokines and promotes atherogenesis (Li et al., 2003; Chen et al., 2005; Mattaliano et al., 2009; Thakkar et al., 2015). Molecular factors regulating LOX-1 stability and signaling functions remain poorly defined. Proteolytic cleavage of LOX-1 liberates a soluble form of this receptor (sLOX-1; Murase et al., 2000). Serum levels of sLOX-1 are modulated in cardiovascular disease (Hayashida et al., 2005). However, the proteolytic enzymes responsible for this have remained controversial (Murase et al., 2000; Mitsuoka et al., 2009; Zhao et al., 2011). Furthermore, the function of the individual cleavage fragments and the impact of proteolysis on LOX-1 signaling are undefined to date.

¹Institute of Physiological Chemistry, Technische Universität Dresden, Dresden, Germany; ²Biochemical Institute, Christian Albrechts University of Kiel, Kiel, Germany; ³Department of Pathology, Cardiovascular Research Institute, Maastricht University, Maastricht, Netherlands; ⁴Systematic Proteome Research and Bioanalytics, Institute for Experimental Medicine, Christian Albrechts University of Kiel, Kiel, Germany; ⁵Department of Molecular Genetics, Cardiovascular Research Institute, Maastricht University, Maastricht, Netherlands; ⁶Amsterdam Cardiovascular Sciences, Department of Medical Biochemistry, Amsterdam University Medical Center, University of Amsterdam, Amsterdam, Netherlands; ⁷German Center for Neurodegenerative Diseases (DZNE), Munich, Germany; ⁸Biomedical Center, Metabolic Biochemistry, Ludwig Maximilians University of Munich, Munich, Germany.

Correspondence to Bernd Schröder: bernd.schroeder@tu-dresden.de; A. Fukumori's present address is Department of Aging Neurobiology, National Center for Geriatrics and Gerontology, Obu and Department of Mental Health Promotion, Osaka University Graduate School of Medicine, Toyonaka, Japan.

© 2019 Mentrup et al. This article is distributed under the terms of an Attribution-Noncommercial-Share Alike-No Mirror Sites license for the first six months after the publication date (see <http://www.rupress.org/terms/>). After six months it is available under a Creative Commons License (Attribution-Noncommercial-Share Alike 4.0 International license, as described at <https://creativecommons.org/licenses/by-nc-sa/4.0/>).

Proteolysis of transmembrane proteins is a well-established mechanism to control their abundance and function (Lichtenthaler et al., 2011). In a sequential process, referred to as regulated intramembrane proteolysis, a cleavage within the substrate's ectodomain is followed by the action of an intramembrane-cleaving protease (I-CLIP) processing the residual membrane-embedded stub. The resulting intracellular domain (ICD) is released into the cytosol and can fulfil regulatory functions like in Notch signal transduction (De Strooper et al., 1999).

Signal peptide peptidase-like 2a and b (SPPL2a, SPPL2b) are I-CLIPs functioning in such regulated intramembrane proteolysis sequences (Voss et al., 2013) by cleaving N-terminal fragments (NTFs) derived from type II transmembrane proteins. They are GxGD-type aspartyl I-CLIPs with homology to presenilins (Voss et al., 2013). SPPL2a and SPPL2b exhibit divergent subcellular localizations in lysosomes/late endosomes and at the plasma membrane (Friedmann et al., 2006; Behnke et al., 2011; Schneppenheim et al., 2014b). While most substrates identified to date have been analyzed in cell-based systems, *in vivo* relevance was shown for SPPL2a-mediated cleavage of the invariant chain (CD74) of the MHCII complex, which is an essential process in development of B cells and dendritic cells documented by a deficiency of these cell types in SPPL2a-deficient mice (Beisner et al., 2013; Bergmann et al., 2013; Schneppenheim et al., 2013). In contrast, the *in vivo* function of SPPL2b is less clear, and evidence for SPPL2b substrates under endogenous conditions is still lacking.

Here, we show that proteolytic pathways regulate the signaling function of LOX-1. Lysosomal proteolysis and ectodomain shedding contribute to the generation of membrane-bound LOX-1 NTFs, which are capable of inducing ligand-independent pro-atherogenic and pro-fibrotic signaling. We demonstrate that levels of the LOX-1 NTFs are controlled by SPPL2a/b, accounting for enhanced LOX-1 signaling in the absence of these proteases. Concomitantly, mice with SPPL2a/b deficiency in non-hematopoietic cells are more susceptible to the development of atherosclerotic plaques. Therefore, we identify SPPL2a/b as essential negative regulators of LOX-1 signaling as well as of atherosclerosis.

Results

LOX-1 is processed by ADAM10 and lysosomal proteases

Based on the described soluble form of LOX-1, we investigated proteolytic processing of this protein in more detail. When we expressed N-terminally HA (hemagglutinin) epitope-tagged murine LOX-1 in HeLa (Fig. 1 A) or immortalized murine aortic endothelial cells (iMAECs; Fig. 1 B), we observed the full-length LOX-1 protein (FL) as well as two hitherto unknown fragments of ~25 and 17 kD, which we termed NTF1 and NTF2. Based on the potential glycosylation of NTF1 suggested by its diffuse band, the two N-glycosylation sites N72 and N92 in the stalk domain (Fig. S1 A) were substituted by alanines (Fig. 1 C). Mutation of N72 led to a shift of NTF1, but not of NTF2, indicating that NTF2 does not contain N72. In contrast, blocking glycosylation at N92 did not alter the migration of any of the NTFs, affecting, however, that of the LOX-1 full-length protein. This

indicates that NTF1 and NTF2 represent distinct proteolytic fragments. Whereas NTF1 is generated by proteolysis between N72 and N92, the cleavage leading to NTF2 has to occur N-terminally to N72.

With regard to previous reports (Mitsuoka et al., 2009; Zhao et al., 2011), we assessed the role of ADAM proteases in LOX-1 processing using HEK cells deficient for ADAM10 and/or ADAM17 (Fig. 1, D and E). The release of sLOX-1 was completely abolished in cells lacking ADAM10, while absence of ADAM17 had no influence on this process. In line, the production of sLOX-1 in iMAECs was stimulated by ionomycin, an ADAM10 activator, but not by PMA, which stimulates ADAM17 (Fig. 1 F). Even in ADAM10 KO cells, no LOX-1 shedding upon PMA treatment was observed (Fig. S1 B). Unexpectedly, the abolished shedding only led to a minor reduction of both NTFs (Fig. 1, D–F) arguing for additional proteolytic pathways for NTF generation. To define these, we tested a panel of protease inhibitors. Bafilomycin A1, an inhibitor of lysosomal acidification, significantly reduced levels of both NTFs (Fig. 1, G and H; and Fig. S1 C). This pointed to a role of pH-dependent lysosomal proteases in LOX-1 processing. In agreement, we observed a partial colocalization of overexpressed LOX-1 with the lysosomal protein LAMP-2 (Fig. 1 I). Furthermore, the cysteine protease inhibitor E-64d caused a reduction of NTF2 (Fig. S1 C). Interestingly, in this case NTF1 was not depleted, but rather stabilized. Thus, multiple lysosomal proteases are involved in the generation of NTF1 and NTF2. Importantly, NTF-production was not influenced by the LOX-1 ligand oxLDL (Fig. 1, K and L), arguing for a constitutive internalization of the receptor followed by proteolytic degradation in lysosomal compartments. Conversely, inhibiting LOX-1 processing influenced neither oxLDL uptake (Fig. S1 D) nor LOX-1 surface levels (Fig. S1 E).

LOX-1 NTFs undergo intramembrane cleavage by SPPL2a/b

We hypothesized that the LOX-1 NTFs are further processed by intramembrane proteases. Based on their topology and localization, we considered SPPL2a and SPPL2b as candidate I-CLIPs. Co-expression of LOX-1 with either protease, but not their catalytically inactive mutants led to a significant reduction of both NTFs that could be blocked with the SPP/SPPL inhibitor (Z-LL)₂-ketone (ZLL; Fig. 2 A). However, NTF depletion induced by SPPL2b was more pronounced (Fig. 2 B). Upon SPPL2a/b coexpression with LOX-1, a smaller band presumably representing the released LOX-1 ICD was enhanced. Immunofluorescence analysis confirmed overlapping distributions between the substrate and both proteases (Fig. 2 C).

We investigated if LOX-1 NTFs are also substrates of endogenous SPPL2a/b proteases. In LOX-1 expressing iMAECs, ZLL stabilized both LOX-1 NTFs (Fig. 2, D and E). Similarly, when analyzing LOX-1 processing in WT and SPPL2a/b double-deficient (dKO) MEF cells, levels of both NTFs were significantly higher in the KO cells (Fig. 2, F and G). We aimed to delineate the individual contributions of SPPL2a and SPPL2b and included SPPL2a and SPPL2b single-deficient MEF cells. Though a minor increase of the LOX-1 NTF1 was observed in SPPL2b^{-/-} MEFs, only the combined ablation of SPPL2a and SPPL2b led to the described major stabilization of LOX-1 NTF2, arguing for a

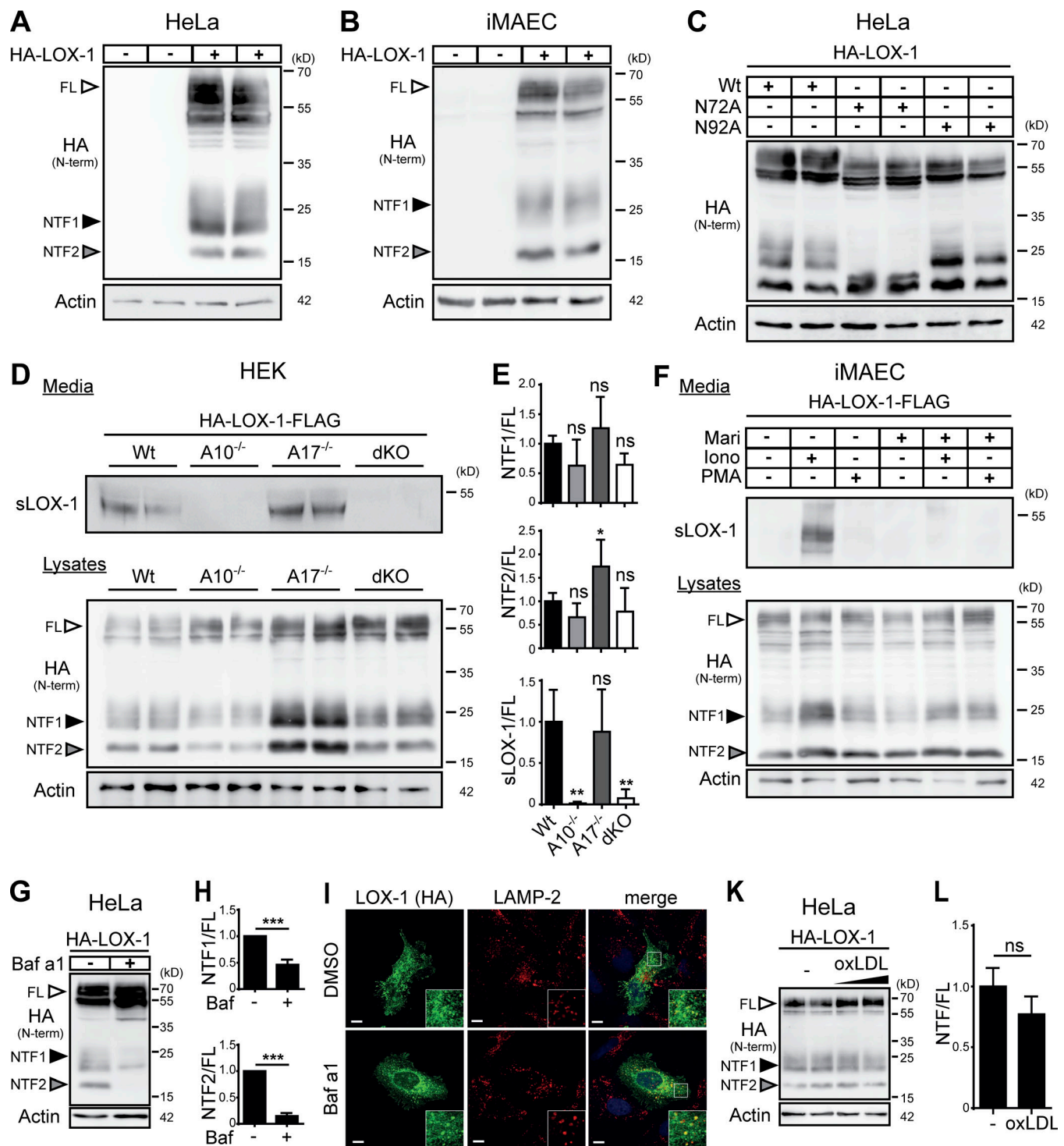


Figure 1. LOX-1 NTFs are generated by ADAM10 and lysosomal proteases. (A and B) Two LOX-1 NTFs were detected by Western blotting upon overexpression of HA-LOX-1 in either HeLa (A) or iMAEC (B) cells. (C) Usage of the potential glycosylation sites at N72 or N92 was analyzed in HeLa cells using respective mutants. (D) HEK cells deficient for ADAM10, ADAM17, or both and WT cells were transfected with HA-LOX-1-FLAG. sLOX-1 was recovered from conditioned media after 16 h by TCA precipitation. (E) Quantification of D. N = 2–3, n = 4–6. One-way ANOVA with Dunnett's post hoc test. (F) iMAECs stably expressing HA-LOX-1-FLAG were preincubated for 2 h in serum-free DMEM containing 10 μM marimastat (Mari) or DMSO. Cells were treated for 30 min with 1 μM ionomycin (Iono) or 100 nM PMA. Cell lysates and conditioned media were analyzed as in D. (G) Lysosomal processing of HA-LOX-1 was blocked in HeLa cells by incubation with 100 nM bafilomycin a1 (Baf a1) for 24 h. (H) Quantification of G. N = 3, n = 3. Student's *t* test. (I) Delivery of HA-LOX-1 to LAMP-2-positive compartments was visualized by indirect immunofluorescence in HeLa cells treated with either DMSO or 100 nM bafilomycin a1 for 6 h. Bars, 10 μm. (J) HA-LOX-1-expressing HeLa cells were treated for 4 h with 40 or 80 μg/ml oxLDL, and NTF formation was analyzed by Western blotting. (K) Quantification of NTF1+2/FL ratios of cells treated with 40 μg/ml oxLDL. N = 2, n = 4. Student's *t* test. ***, *P* ≤ 0.001; **, *P* ≤ 0.01; *, *P* ≤ 0.05; ns, not significant. N, the number of independent experiments; n, the number of individual samples for quantification. All data are shown as mean ± SD.

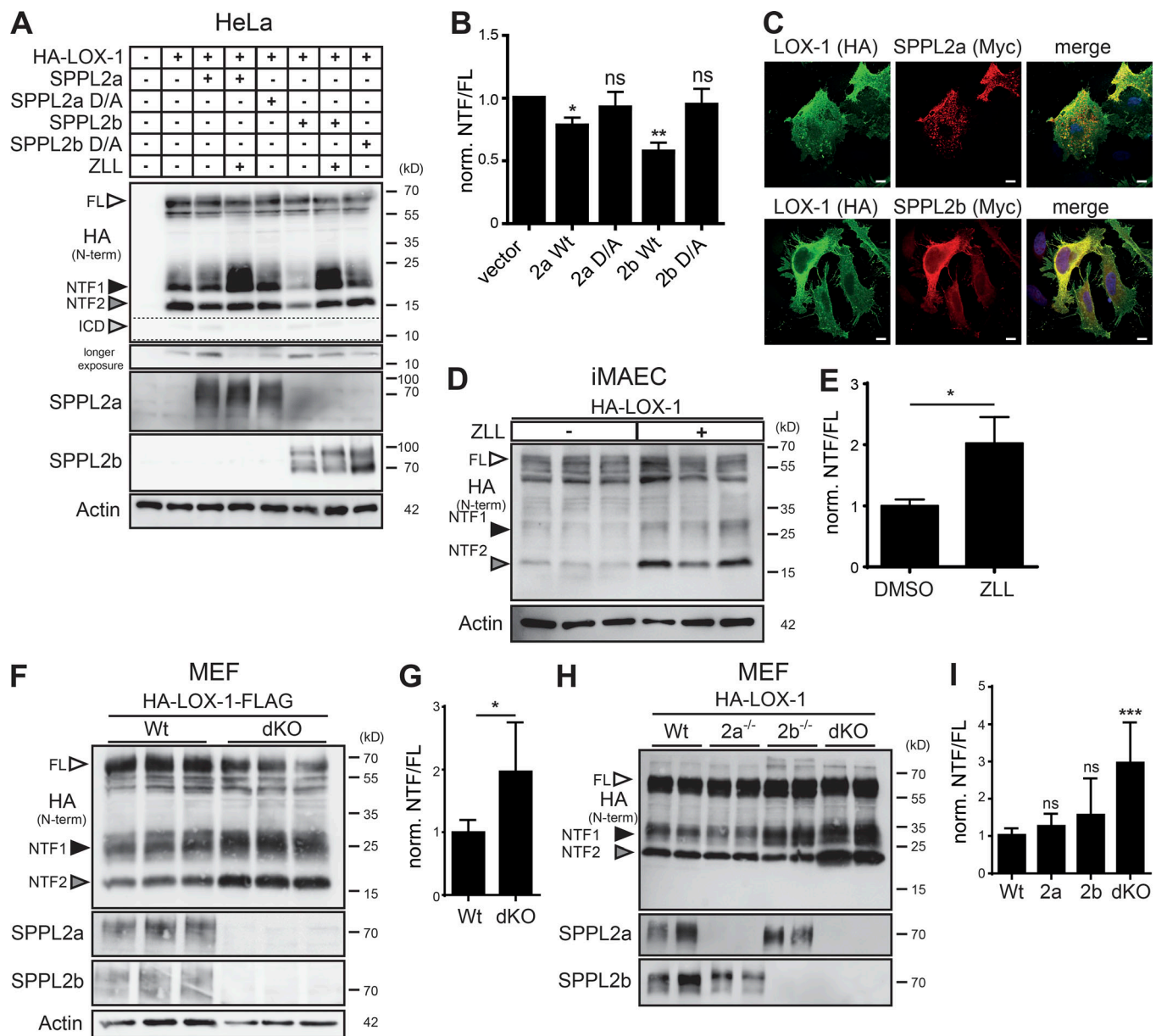


Figure 2. LOX-1 NTFs undergo SPPL2a/b-dependent intramembrane proteolysis. (A) HeLa cells were transfected with HA-LOX-1 and WT or inactive (D/A) SPPL2 proteases. Where indicated, SPPL2a/b activity was inhibited with 20 μ M ZLL for 6 h. **(B)** Quantification of A. N = 7, n = 7. Student's *t* test. Norm., normalized. **(C)** Colocalization of HA-LOX-1 and SPPL2a-myc or SPPL2b-myc in transfected HeLa cells. **(D and E)** iMAECs transfected with HA-LOX-1 were treated with 40 μ M ZLL for 24 h before Western blot analysis. LOX-1 (NTF1+2)/FL ratios are depicted in E. N = 2, n = 5. Student's *t* test. **(F and G)** WT or SPPL2a/b dKO MEFs were stably transduced with HA-LOX-1-FLAG followed by Western blot analysis. LOX-1 (NTF1+2)/FL ratios are depicted in G. N = 2, n = 6. Student's *t* test. **(H)** WT, SPPL2a^{-/-}, SPPL2b^{-/-}, or double-deficient MEFs were transfected with HA-LOX-1 and analyzed by Western blotting. **(I)** Quantification of H. N = 3–4, n = 5–8. One-way ANOVA with Tukey's post hoc testing. ***, *P* ≤ 0.001; **, *P* ≤ 0.01; *, *P* ≤ 0.05; ns, not significant. N, the number of independent experiments; n, the number of individual samples for quantification. All data are shown as mean ± SD.

synergistic role of endogenous SPPL2a/b in LOX-1 processing (Fig. 2, H and I).

We wanted to confirm that the effect of SPPL2a/b on LOX-1 NTFs represents proteolysis within the transmembrane domain (TMD). Therefore, we expressed a LOX-1 model NTF (Fig. 3 A) comprising amino acids 1–88 together with SPPL2a or SPPL2b in HEK cells and recovered the C-terminal cleavage products for mass-spectrometric analysis from the media. To avoid heterogeneity by N-glycosylation, we mutated the N-glycosylation

site at N72. We observed six specific cleavage fragments (Fig. 3 B) that were not present in control samples (Fig. S1 F). The determined peaks were matched with theoretical masses calculated for C-terminal peptides based on the NTF sequence (Fig. 3 C). Both proteases exhibited multiple overlapping cleavage sites within the TMD of LOX-1. Interestingly, SPPL2a showed a strong preference for proteolysis N-terminal to L52, whereas the predominant site used by SPPL2b was shifted to I53.

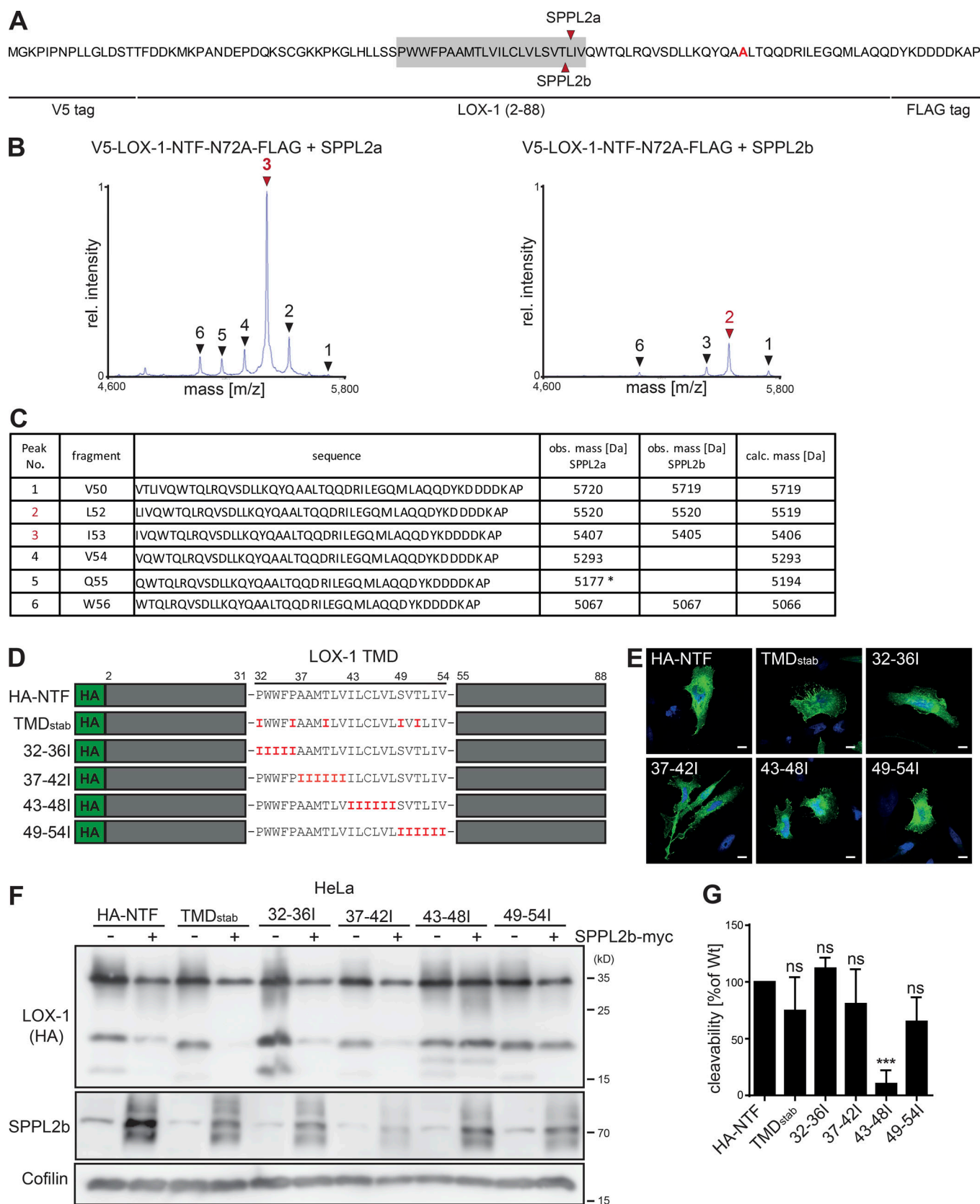


Figure 3. The LOX-1 TMD is important for SPPL2-dependent intramembrane cleavage. (A–C) Mass-spectrometric determination of SPPL2a/b cleavage sites within the LOX-1 NTF. **(A)** Amino acid sequence of the employed model substrate. Determined cleavage sites in the TMD (gray) are marked. **(B)** Secreted C-terminal fragments were purified from conditioned media and analyzed by MS. Arrows indicate peptides increased by protease overexpression with the predominant peaks labeled in red. **(C)** Peptides assigned to the respective peaks shown in B. Peak 5 corresponds to a peptide with a potential N-terminal

glutamate to pyroglutamate conversion. obs., observed; calc., calculated. **(D)** Scheme of LOX-1 NTF TMD mutants. **(E)** Subcellular sorting of LOX-1 TMD mutants was compared with the WT LOX-1 NTF by indirect immunofluorescence with anti-HA in HeLa cells. Bar, 10 μ m. **(F)** Cleavage of LOX-1 NTF TMD mutants by SPPL2b was analyzed in transfected HeLa cells. **(G)** Quantification of F. N = 4, n = 4. One-way ANOVA with Dunnett's post hoc test. ***, $P \leq 0.001$; ns, not significant. N, the number of independent experiments; n, the number of individual samples for quantification. All data are shown as mean \pm SD.

We aimed to identify determinants within the LOX-1 TMD required for the intramembrane cleavage. Based on the role of helix destabilization for intramembrane proteolysis (Langosch et al., 2015), we tried to increase the stability of the LOX-1 TMD by replacing either selected polar or helix-destabilizing residues (TMD_{stab}) or blocks of amino acids (32–36I, 37–42I, 43–48I, 49–54I) with isoleucines (Fig. 3 D). All mutants reached the plasma membrane like the LOX-1 WT NTF (Fig. 3 E). Whereas processing of most mutants by coexpressed SPPL2b was not compromised, exchange of residues 43–48 significantly impaired intramembrane cleavage (Fig. 3 F and G). Interestingly, the residues surrounding the cleavage sites between T51, L52, and I53 could be replaced without a significant loss of cleavability.

Endogenous LOX-1 is a substrate of SPPL2a and SPPL2b

To analyze endogenous LOX-1, we generated an antiserum against an N-terminal epitope (aa 2–19) of the protein (Fig. 4, A and B). We confirmed endogenous expression of SPPL2a and SPPL2b in iMAECs and aortic lysates (Fig. 4 C) and observed that inhibition of SPP/SPPL proteases stabilized endogenous LOX-1

NTF2 in iMAECs (Fig. 4, D and E). We also analyzed LOX-1 processing in aortae isolated from WT as well as SPPL2a/b single- and double-deficient mice (Fig. 4, F and G). Similar to iMAECs, we exclusively detected NTF2 in these samples. Only minor amounts of LOX-1 NTF2 were detected in WT aortae, whereas those from dKO mice exhibited a major accumulation. In both the single-deficient aortae, NTF2 abundance was increased. However, levels were much lower than in the dKO aortae, strongly highlighting the importance of both proteases for LOX-1 processing in vivo.

Inhibition of SPPL2a/b enhances ligand-dependent LOX-1-induced MAP kinase signaling

We assessed the impact of SPPL2a/b-mediated LOX-1 proteolysis on the signaling of this receptor. Therefore, we generated an inducible LOX-1-expressing HEK cell line (Fig. 5 A). Treatment with oxLDL triggered phosphorylation of the MAP kinases ERK1/2 (pERK) only when LOX-1 expression was induced (Fig. 5 B). Importantly, inhibition of SPPL2a/b enhanced ERK activation (Fig. 5, B and C). This effect was recapitulated in ZLL-treated

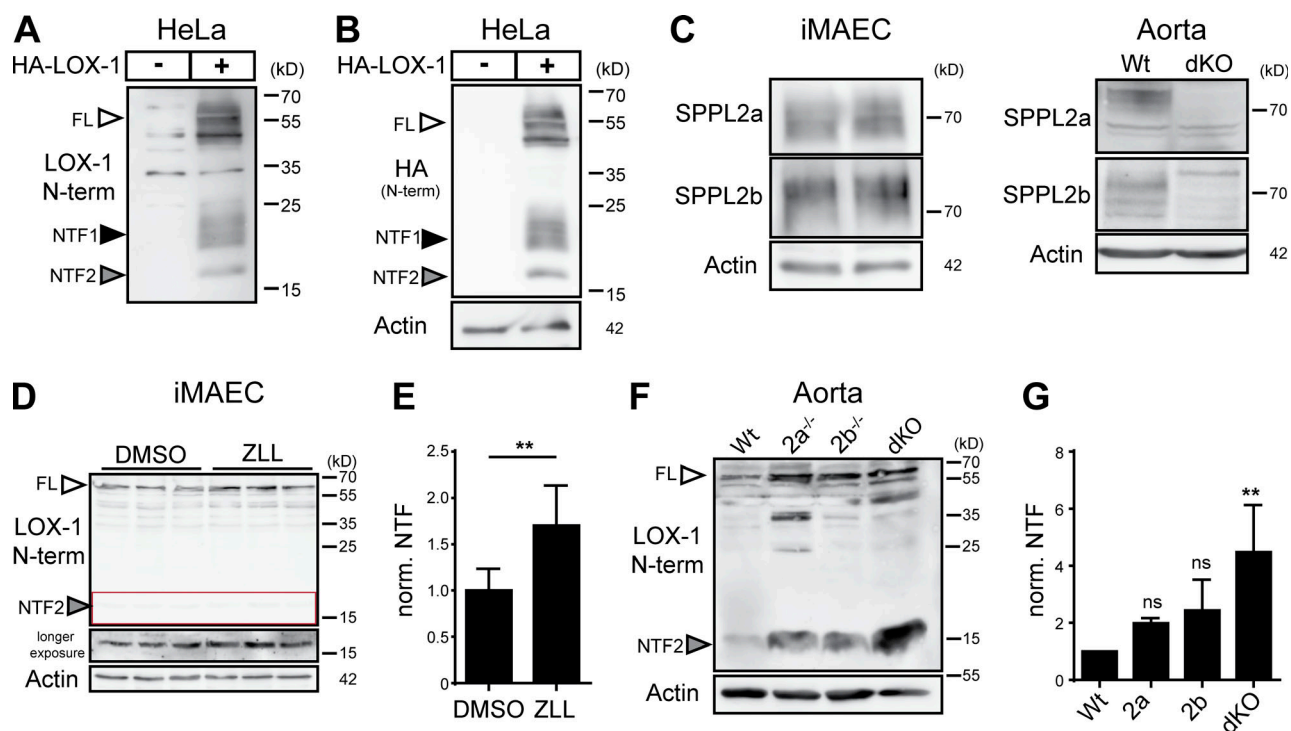


Figure 4. **Endogenous LOX-1 is processed by SPPL2a and SPPL2b.** **(A and B)** Evaluation of functionality of the newly generated antibody against the N terminus of murine LOX-1 in transfected HeLa cells. **(A)** Blot probed with new antibody. **(B)** Same blot as in A probed with anti-HA. **(C)** Expression of SPPL2a and SPPL2b was demonstrated in iMAECs and aortic lysates by Western blotting. **(D)** iMAECs were treated for 24 h with either 40 μ M ZLL or DMSO before Western blot analysis. **(E)** Quantification of D. N = 2, n = 6. Student's t test. **(F)** LOX-1 NTF levels were analyzed in aortic lysates from WT, SPPL2a^{-/-}, SPPL2b^{-/-}, or dKO mice by Western blotting. **(G)** Quantification of F. N = 4, n = 4. One-way ANOVA with Tukey's post hoc testing. **, $P \leq 0.01$; ns, not significant. N, the number of independent experiments; n, the number of individual samples for quantification. All data are shown as mean \pm SD.

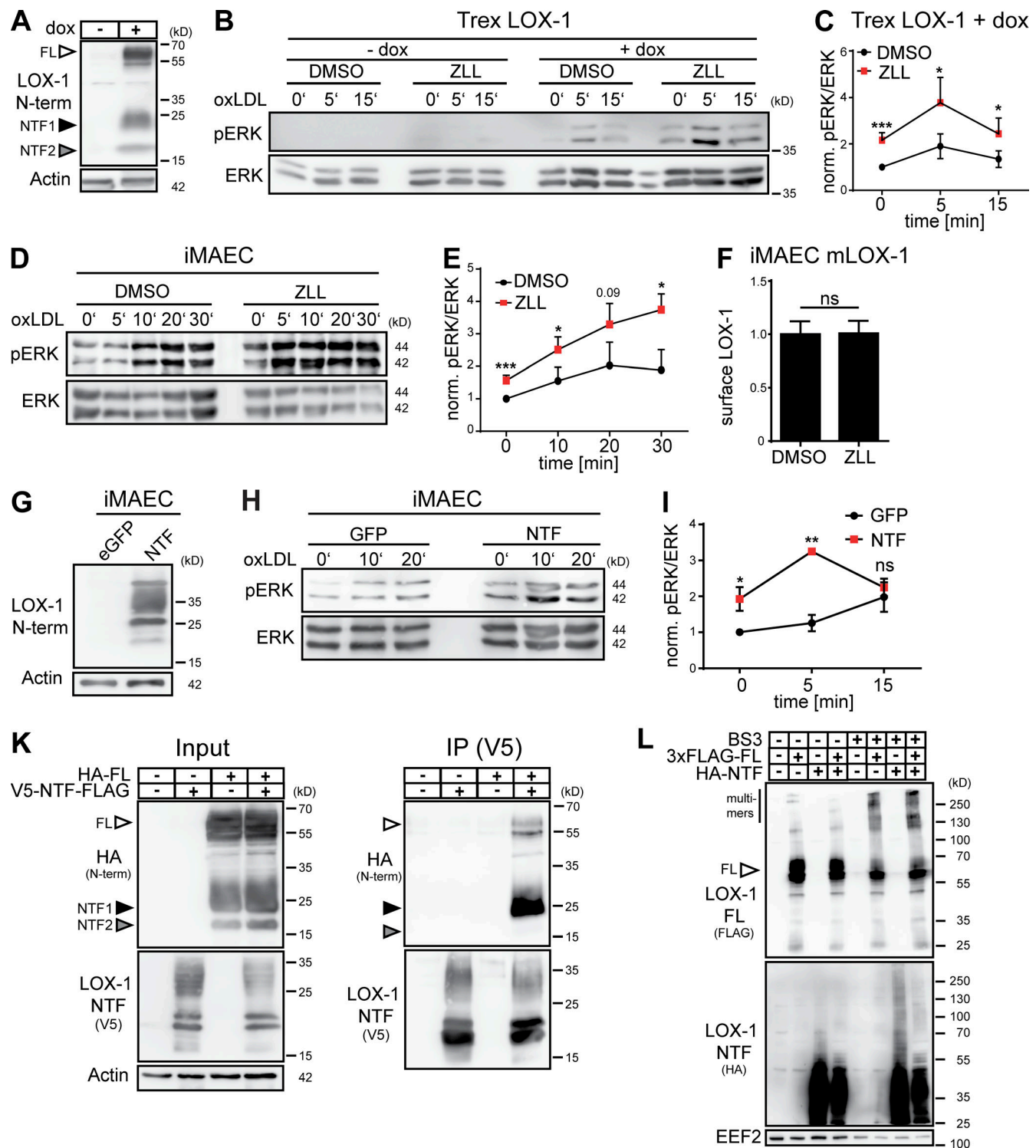


Figure 5. The LOX-1 NTF regulates MAP kinase activity. (A) T-Rex FlpIn cells inducibly overexpressing LOX-1 were generated. LOX-1 expression after induction with 10 μ g/ml doxycycline (dox) for 24 h was confirmed by Western blotting. (B) LOX-1 expression was induced in T-Rex FlpIn cells (+dox) or cells were left uninduced (-dox). Prior to stimulation with 40 μ g/ml oxLDL, cells were cultured in serum-free DMEM for 4 h in the presence of 40 μ M ZLL or DMSO. pERK and total ERK1/2 (ERK) levels were determined. (C) Quantification of B. N = 4, n = 4. Student's *t* test. (D) iMAECs were incubated with 40 μ M ZLL or DMSO for 24 h. For the last 4 h, cells were transferred to serum-free DMEM before treatment with 40 μ g/ml oxLDL and analysis of ERK1/2 activation. (E) Quantification of D. N = 4, n = 4. Student's *t* test. (F) LOX-1 surface levels were analyzed by flow cytometry in iMAECs stably overexpressing LOX-1 after 24 h treatment with 40 μ M ZLL. N = 2, n = 6. Student's *t* test. (G) Stable expression of the LOX-1 NTF in transduced iMAECs was validated. (H) Transduced iMAECs were cultivated for 4 h under serum-free conditions before stimulation with 40 μ g/ml oxLDL and assessment of MAP kinase activation. (I) Quantification of H. N = 3, n = 3. Student's *t* test. (K) HeLa cells were transfected as indicated with differentially tagged full-length LOX-1 and NTF. Interaction of both proteins was analyzed by coimmunoprecipitation using anti-V5. (L) HeLa cells transfected with 3xFLAG-LOX-1 (3xFLAG-FL) and/or HA-LOX-1₁₋₈₈

(HA-NTF) were treated for 30 min with BS³ and subsequently analyzed by Western blotting. As described in Materials and methods, phosphorylated and total forms of ERK were detected from the same membranes. After detection of pERK, the respective membranes were stripped and reprobed to detect total ERK. ***, $P \leq 0.001$; **, $P \leq 0.01$; *, $P \leq 0.05$; ns, not significant. N, the number of independent experiments; n, the number of individual samples for quantification. All data are shown as mean \pm SD.

iMAECs (Fig. 5, D and E). Based on endogenous LOX-1 expression in this cell type, this substantiates that SPPL2a/b negatively regulate LOX-1 signaling. We hypothesized that enhanced LOX-1 signaling upon SPPL2a/b inhibition could be caused by increased presence of LOX-1 at the cell surface. Since we failed to detect endogenous LOX-1 in iMAECs by flow cytometry, we quantified LOX-1 surface levels in iMAECs overexpressing LOX-1 upon treatment with ZLL, which were not changed compared with controls (Fig. 5 F).

Since SPPL2a/b inhibition or deficiency induces accumulation of LOX-1 NTFs (Fig. 4, D–G), we considered a direct role of these fragments in enhancing LOX-1 signaling. Therefore, we stably expressed an untagged LOX-1 NTF in iMAECs (Fig. 5 G) and compared ERK phosphorylation in response to oxLDL to control cells (Fig. 5 H). In NTF-expressing cells, oxLDL-induced ERK activation was strongly augmented (Fig. 5 I) phenocopying SPPL2a/b inhibition (Fig. 5, D and E). We postulated a molecular interaction between this fragment and full-length LOX-1, which was confirmed by coimmunoprecipitation in transfected HeLa cells (Fig. 5 K). LOX-1 can form oligomers depending on receptor density (Matsunaga et al., 2007). Oligomerization was found to positively correlate with ligand binding. We evaluated if presence of the NTF increases LOX-1 oligomers which can be cross-linked in HeLa cells expressing LOX-1 full-length and/or the NTF. Despite minor changes in the band pattern, the overall amount of LOX-1 full-length oligomers was not considerably modulated by the NTF (Fig. 5 L), questioning the relevance of the described NTF–full-length LOX-1 interaction for the enhanced signaling.

The LOX-1 NTF activates MAP kinases independent of LOX-1 ligands

We noticed that in NTF-expressing iMAECs ERK activation was already significantly increased before the addition of oxLDL (Fig. 5, H and I). We analyzed further signaling pathways in unstimulated iMAECs overexpressing the LOX-1 NTF (Fig. 6, A–C). In addition to ERK, activation of p38 MAP kinase was significantly enhanced. In contrast, we did not detect increased phosphorylation of the NF κ B subunit p65 or the kinase AKT. Thus, the LOX-1 NTF triggers a specific ligand-independent MAP kinase activation. To validate the ligand independence, we re-analyzed NTF-expressing iMAEC and control cells after serum deprivation. Increased levels of pERK and p38 were preserved under these conditions (Fig. 6, D and E). We repeated these experiments in HEK cells. Like in iMAECs, expression of the LOX-1 NTF significantly increased basal activation of ERK and p38. No effects on Akt and p65 were observed (Fig. 6, F and G). In HEK cells, endogenous LOX-1 expression was in the range of the detection limit of the performed quantitative RT-PCR (qRT-PCR; data not shown). Therefore, MAP kinase activation by the LOX-1 NTF can be considered independent of the full-length receptor.

Several upstream pathways are involved in LOX-1 NTF induced MAP kinase activation

We aimed to delineate the pathways triggered by the LOX-1 NTF responsible for MAP kinase activation in iMAECs (Fig. 6, H–L). Inhibition of MEK1/2 by U0126 potentially reduced activation of ERK, however, had no significant impact on p38. In addition, we also assessed inhibitors against Src family as well as Rho-associated protein kinases (ROCKs). Whereas inhibition of Src kinases impaired activation of both ERK and p38, ROCK inhibition only affected the latter. Thus, not a single, but multiple upstream pathways mediate MAP kinase activation by the LOX-1 NTF. We aimed to identify the molecular determinants within the LOX-1 NTF required for the signaling activation. We mutated all phosphorylatable residues within the cytoplasmic domain of the NTF (Fig. 6 M). However, this mutant was not compromised with regard to MAP kinase activation (Fig. 6, N and O). Furthermore, we evaluated the signaling potential of the isoleucine transmembrane mutants. Surprisingly, their capability to induce signaling was significantly reduced (Fig. 6, P and Q), pointing to a critical role of the TMD, which could act as interaction interface. Based on the described NTF full-length interaction, we tested the ability of the LOX-1 NTF for homophilic interactions. Differentially tagged WT LOX-1 NTFs could be efficiently coimmunoprecipitated. This interaction was abolished with any of the four TMD mutants (Fig. 6, R and S), indicating that the ability of the NTF to undergo homo- and/or heterophilic protein–protein interactions via the TMD is critical for MAP kinase activation.

LOX-1 NTF triggered signaling induces pro-atherogenic and -fibrotic targets

A well-established downstream effect of LOX-1 activation is the up-regulation of adhesion molecules like ICAM-1 (Chen et al., 2005; Inoue et al., 2005). Western blotting revealed a significant increase of ICAM-1 in NTF-overexpressing iMAECs (Fig. 7, A and B). This was also reflected in higher ICAM-1 levels at the cell surface (Fig. 7 C) in a similar range as induced by TNF. Importantly, also *Icam1* mRNA was increased (Fig. 7 D), indicating that the LOX-1 NTF acts by enhancing *Icam1* expression.

We screened for further targets influenced by NTF overexpression in the same system using qRT-PCR-based arrays (Table S1). 11 targets were selected for further validation (Fig. 7, E and F). We could confirm a significant up-regulation of the chemokine *Cxcl2*, the CASP8 and FADD-like apoptosis regulator *Cflar*, the connective tissue growth factor *Ctgf*, the granulocyte-macrophage colony-stimulating factor *Csf2*, and the platelet-derived growth factor subunit B *Pdgfb* in iMAECs overexpressing the LOX-1 NTF. In contrast, mRNA levels of the platelet factor 4 *Pf4* were significantly reduced. In case of CTGF, we confirmed enhanced production of this secreted protein by Western blot analysis of Brefeldin A-treated cells (Fig. 7, G and H).

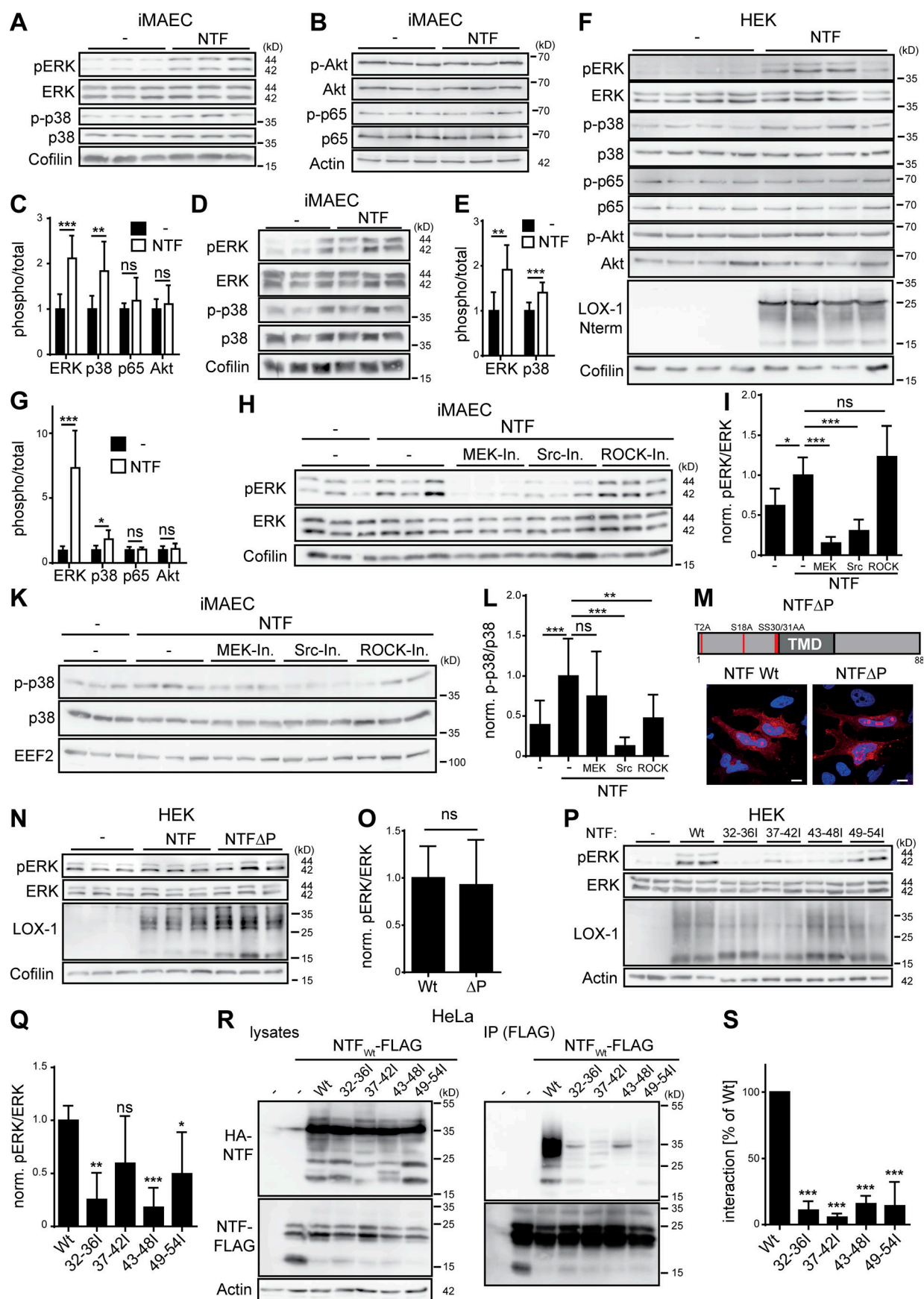


Figure 6. The LOX-1 NTF autonomously activates MAP kinases. (A and B) iMAECs were stably transduced with the pMSCV puro vector (–) or a LOX-1-NTF coding construct. Levels of phosphorylated as well as total ERK1/2, p38 (A), p65, and Akt (B) were analyzed by Western blotting. (C) Quantification of A and B. $N = 3$, $n = 9$. Student's t test. (D) Control or NTF-transduced iMAECs were starved for 16 h in serum-free DMEM and subsequently analyzed for activation of MAP kinases. (E) Quantification of D. $N = 2$, $n = 6$. Student's t test. (F) Vector (–) or LOX-1 NTF transfected HEK cells were selected with puromycin for 4 d. (G) Quantification of F. $N = 2$, $n = 7$. Student's t test. (H) Empty vector (–) or LOX-1 NTF transduced iMAECs were treated for 3 h with 25 μ M U0126 (MEK-Inh.), 1 μ M Saracatinib (Src-Inh.), or 10 μ M Y-27632 (ROCK-Inh.) and subsequently analyzed for ERK1/2 activation. (I) Quantification of H. $N = 2$, $n = 6$. One-way ANOVA with Tukey's post hoc test. (J) Pathways upstream of p38 MAP kinase activation were assessed as depicted in H. (L) Quantification of K. $n = 4$, $n = 12$. One-way ANOVA with Tukey's post hoc test. (M) Subcellular sorting of an unphosphorylatable LOX-1 NTF (NTF Δ P) was compared with the WT NTF by indirect immunofluorescence in HeLa cells. Bars, 10 μ m. (N) HEK cells were transfected and incubated for 4 d with 10 μ g/ml puromycin. Activation of ERK1/2 was monitored by Western blotting. (O) Quantification of N. pERK/ERK levels were normalized (norm.) to LOX-1 NTF expression. $N = 2$, $n = 6$. Student's t test. (P) Induction of pERK by LOX-1 TMD mutants was analyzed by Western blotting. (Q) pERK/ERK ratios were normalized to NTF expression. $N = 3$, $n = 6$. One-way ANOVA with Dunnett's post hoc test. (R) Coimmunoprecipitation of the HA-tagged NTF mutants with a FLAG-tagged WT LOX-1 NTF from lysates of transfected HEK cells. (S) Quantification from $N = 3$, $n = 3$ experiments. One-way ANOVA with Dunnett's post hoc test. As described in Materials and methods, phosphorylated and total forms of ERK, p38, p65, and Akt were detected from the same membranes. After detection of the phosphorylated forms, membranes were stripped and reprobed to detect the total proteins. ***, $P \leq 0.001$; **, $P \leq 0.01$; *, $P \leq 0.05$; ns, not significant. N , the number of independent experiments; n , the number of individual samples for quantification. All data are shown as mean \pm SD.

We assessed the relevance of the described signaling pathways for the identified transcriptional regulation. Therefore, we determined the effect of MEK, Src, and ROCK inhibition on the up-regulation of *Icam1* (Fig. 7 I), *Pdgfb* (Fig. 7 K), and *Ctgf* (Fig. 7 L). Whereas ROCK inhibition significantly counteracted the increase of *Icam1* expression, none of the other compounds had significant effects on this target. In contrast, Src inhibition effectively reduced mRNA levels of *Pdgfb* and *Ctgf*. In addition, the NTF-associated *Ctgf* up-regulation was also responsive to MEK inhibition. Thus, several upstream pathways in individual combinations contribute to the transcriptional effects, highlighting the complexity of the LOX-1 NTF-induced signaling.

Next, we wondered if also an NTF accumulation derived from inhibiting the intramembrane cleavage of endogenous LOX-1 would impact on the identified target genes. Therefore, mRNA levels of the validated targets were determined in ZLL-treated iMAECs and controls. With the exception of *Cflar* and *Pf4*, we observed a significant up-regulation of *Icam1*, *Pdgfb*, *Csf2*, *Ctgf*, and *Cxcl2* upon SPPL2a/b inhibition (Fig. 7 M). We also analyzed ICAM-1 surface levels by flow cytometry and found a significant increase in inhibitor-treated cells (Fig. 7 N). This further confirms that in iMAECs, SPPL2a/b inhibition phenocopies overexpression of the LOX-1 NTF. These findings strongly suggest that SPPL2a/b deficiency induces a pro-atherogenic and pro-fibrotic state in endothelial cells via the accumulation of LOX-1 NTFs.

Enhanced atherosclerosis in SPPL2a/b double-deficient mice

In healthy aortae from WT mice, low levels of the LOX-1 NTF are present (Fig. 4 F), which are increased following induction of atherosclerosis (Fig. S2, A and B). This suggests a need for SPPL2a/b to clear this fragment under such conditions. Therefore, we analyzed if SPPL2a/b deficiency has an impact on the development of atherosclerosis in vivo. We wanted to exclude that the immunological phenotype of SPPL2a/b-deficient (dKO) mice (Schneppenheim et al., 2014b) caused by defective processing of CD74 (Schneppenheim et al., 2013) confounds the analysis. Therefore, dKO and WT mice were reconstituted with WT bone marrow (Fig. S2 C), and recovery of normal hematopoiesis was confirmed by flow-cytometric analysis of blood samples (Fig. S2, D and E). At the end of the experiment, analysis of splenocytes demonstrated a full

correction of the B cell maturation block of the dKO mice (Fig. 8 A and Fig. S2 F).

After recovery from transplantation, hypercholesterolemia was induced by adeno-associated viral overexpression of a PCSK9 gain-of-function mutant in combination with a Western-type high cholesterol diet (HCD; Björklund et al., 2014). This model has been recently established as an effective approach to eliminate LDL receptor molecules from the cell surface, thereby causing hypercholesterolemia comparable to *Ldlr*^{–/–} mice but circumventing the need for genetic ablation of the corresponding gene (Goettsch et al., 2016; Lu et al., 2016; Rogers et al., 2017; Theodorou et al., 2017). In agreement with this, mice of both genotypes developed significant hypercholesterolemia and hypertriglyceridemia (Fig. 8 B). However, plasma cholesterol concentrations in the treated dKO mice were \sim 30% lower than in control mice. Strikingly, even despite lower plasma cholesterol levels, atherosclerotic lesion size was significantly increased in the dKO mice (Fig. 8 C). While plaque macrophage and smooth muscle cell content were not altered between both genotypes, dKO mice displayed a twofold increase in plaque collagen (Fig. 8 C). Furthermore, plaques of these mice had larger necrotic areas than those of controls (Fig. 8 D). Histopathological scoring revealed an increased proportion (52% vs. 36%) of advanced atherosclerotic plaques in dKO animals (Fig. 8 E), highlighting a pro-atherogenic effect of SPPL2a/b deficiency in nonhematopoietic cells in vivo.

We analyzed MAP kinase activation in atherosclerotic aortic arches (Fig. 8 F). In line with the findings in cell-based experiments, phosphorylation of ERK and p38 was significantly enhanced in atherosclerotic aortae from dKO mice (Fig. 8 G). Activation of Akt and NF κ B pathways was similar in samples from both genotypes (Fig. S2 G). In addition, also ICAM-1 was strongly up-regulated in the aortae from dKO mice after atherosclerosis induction (Fig. 8, F and G). Therefore, the cellular phenotypes linked to SPPL2a/b deficiency and enhanced LOX-1 NTF levels in vitro were recapitulated upon induction of atherosclerosis in vivo.

Despite this obvious correlation, an additional impact of further substrates to the atherosclerotic phenotype of SPPL2a/b-deficient mice is in general conceivable. Therefore, we performed Western blot analysis of TNF-activated iMAECs as well

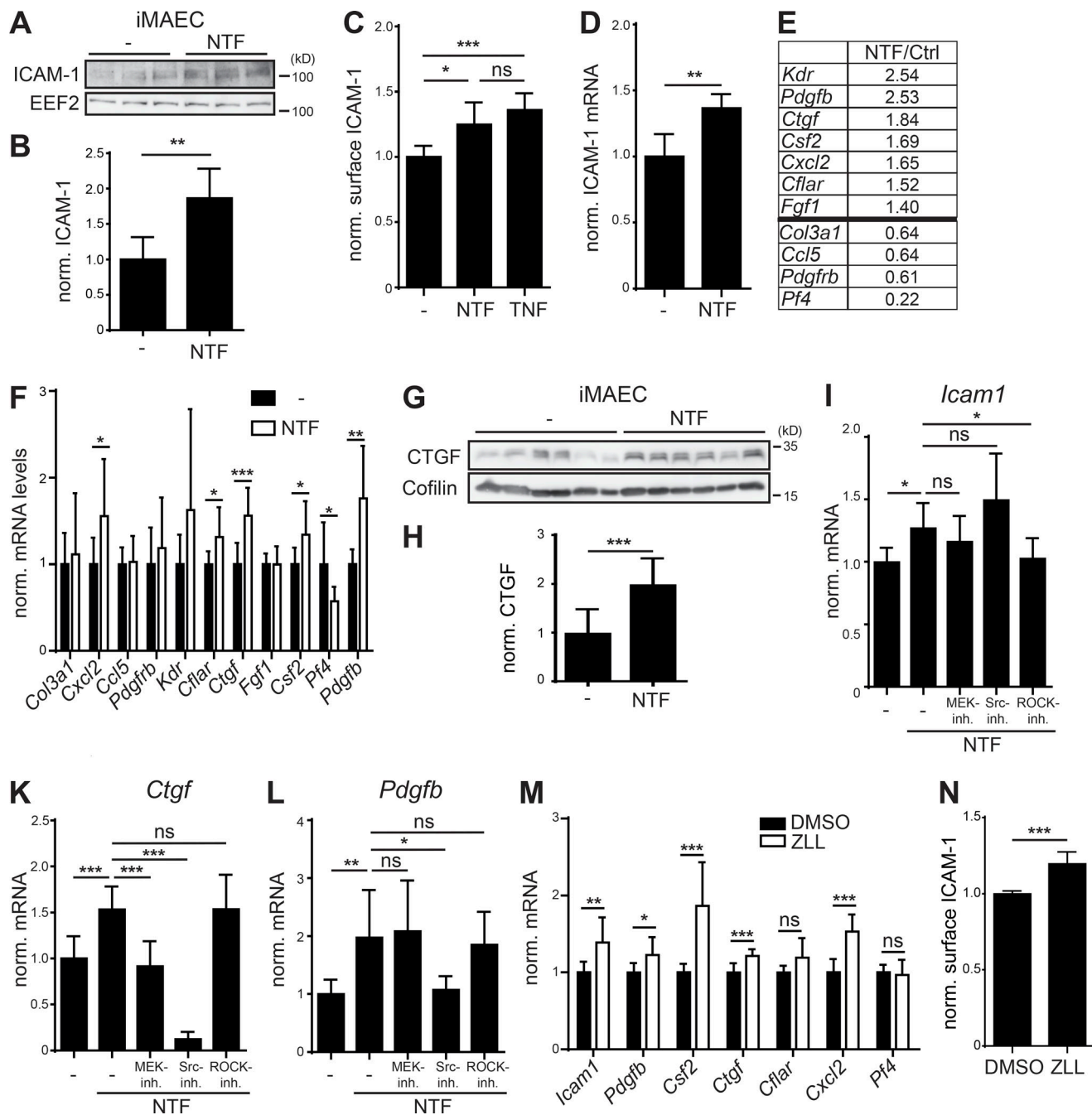


Figure 7. Accumulation of the LOX-1 NTF induces a pro-atherogenic state in endothelial cells. (A) Expression of ICAM-1 was analyzed in control (-) or LOX-1 NTF transduced iMAECs by Western blotting. (B) Quantification of A. $N = 2$, $n = 6$. Student's t test. (C) Up-regulation of surface ICAM-1 in LOX-1 NTF transduced iMAECs was validated by flow cytometry. As a control, cells were treated with 5 ng/ml TNF. $N = 2$, $n = 6$. One-way ANOVA with Tukey's post hoc test. (D) Up-regulation of *Icam-1* was validated by qPCR. $N = 2$, $n = 6$. Student's t test. (E) Candidate genes from endothelial cell biology and atherosclerosis RT² Profiler arrays with differential regulation between control and iMAEC NTF cells. (F) Differences in mRNA levels of the selected genes were validated by qPCR. $N = 2-3$, $n = 6-9$. Student's t test. (G) Secretion of CTGF was blocked in iMAEC control (-) or NTF cells by incubation with Brefeldin A (1 μ g/ml) for 6 h. Intracellular CTGF levels were analyzed by Western blotting. (H) Quantification of G. $N = 2$, $n = 12$. Student's t test. (I-L) iMAEC control or NTF cells were treated for 3 h with 25 μ M U0126 (MEK-Inh.), 1 μ M Saracatinib (Src-Inh.), or 10 μ M Y-27632 (ROCK-Inh.) or left untreated as indicated. *Icam-1* (I, $N = 3-4$, $n = 9-12$), *Ctgf* (K, $N = 3$, $n = 8-9$), and *Pdgfb* (L, $N = 3$, $n = 8-9$) mRNA levels were quantified by qPCR. One-way ANOVA with Dunnett's post hoc test. (M) Up-regulation of validated candidate genes was monitored in iMAECs treated for 16 h with either DMSO or 40 μ M ZLL. $N = 2-3$, $n = 6-9$. Student's t test. (N) Up-regulation of ICAM-1 upon ZLL administration was validated by flow cytometry. $N = 3$, $n = 11$. Student's t test. ***, $P \leq 0.001$; **, $P \leq 0.01$; *, $P \leq 0.05$; ns, not significant. N, the number of independent experiments; n, the number of individual samples for quantification. All data are shown as mean \pm SD.

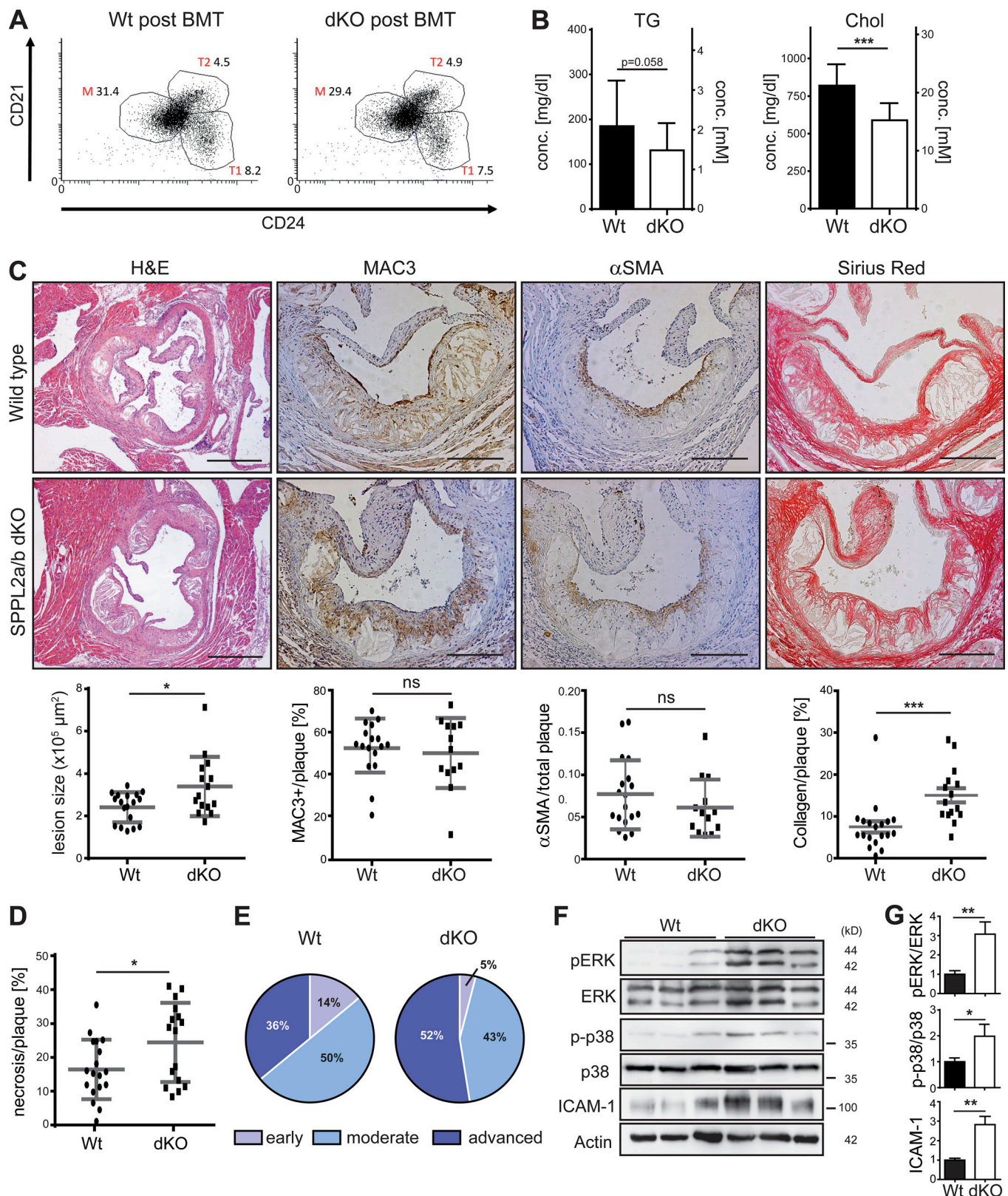


Figure 8. Enhanced atherosclerosis in SPPL2a/b double-deficient mice. (A–G) Hypercholesterolemia and atherosclerosis were induced in WT and SPPL2a/b-deficient (dKO) mice by adeno-associated viral expression of D377Y-mPCSK9 and an HCD for 9 wk following bone marrow transplantation (BMT) with WT bone marrow. (A) Proportions of transitional stage 1 (T1) and 2 (T2) as well as mature B cells (% of viable splenocytes) were analyzed by flow cytometry at the end of the atherosclerosis experiment. The dot plots depict viable B220⁺ splenocytes. (B) Plasma triglyceride (TG) and cholesterol (Chol) levels were determined 3 wk after HCD initiation. N = 2, n = 18–20. (C) Atherosclerotic plaque development was analyzed histologically in H&E-stained aortic root cross-sections. Bars, 400 μ m. Plaque macrophage, smooth muscle cell, and collagen contents were quantified based on MAC3, α SMA (alpha smooth muscle actin),

and Sirius Red staining, respectively. Bars, 200 μ m. N = 2, n = 13–18 (α SMA); n = 13–17 (MAC3), n = 15–18 (size), n = 15–19 (Sirius Red). **(D)** Quantification of necrotic plaque area. N = 2, n = 16–18. **(E)** Scoring of atherosclerotic plaques. **(F)** Activation of ERK1/2 and p38 MAP kinases as well as ICAM-1 levels was compared in atherosclerotic aortae from WT and dKO mice. **(G)** Quantification of pERK/ERK (N = 2, n = 6), p-p38/p38 (N = 4, n = 11–12) and ICAM-1/actin (N = 2, n = 5–6) ratios. As described in Materials and methods, phosphorylated and total forms of ERK and p38 were detected from the same membranes. After detection of pERK and p38, the respective membranes were stripped and reprobed to detect the total proteins. Student's *t* test. ***, $P \leq 0.001$; **, $P \leq 0.01$; *, $P \leq 0.05$; ns, not significant. N, the number of independent experiments; n, the number of individual samples for quantification. All data are shown as mean \pm SD.

as aortae from WT and dKO mice for the best characterized substrates CD74 and TNF. We failed to detect relevant amounts of these proteins in these samples (Fig. S3, A–C). In addition, we performed a quantitative proteomic analysis of aorta from WT and dKO mice (Fig. S3 D and Table S2). We detected 3 known SPPL2a/b substrates and 120 other type II transmembrane proteins as substrate candidates. However, their abundance was not different between both genotypes. Thus, in these approaches we did not obtain evidence for other SPPL2a/b substrates being of pathophysiological importance in endothelial cells and aortae, supporting the critical role of the LOX-1–SPPL2a/b axis.

SPPL2a/b proteases in human atherosclerosis

With regard to the clinical relevance of atherosclerosis, we determined if the pathway identified in mice also has implications for atherosclerosis in humans. Thus, we analyzed proteolytic processing of human LOX-1 (hLOX-1). Upon overexpression in HeLa cells also the human receptor underwent proteolysis leading to the generation of NTFs (Fig. 9, A and B). Here, primarily the smaller NTF2 was detected. We confirmed that NTF2 was efficiently cleaved in particular by coexpressed SPPL2b and also processed by endogenous SPPL proteases (Fig. 9, C and D). In this case, SPPL2a and SPPL2b shared a major cleavage site C-terminal to M54 (Fig. 9, E–G). In addition, SPPL2b also cleaved efficiently C-terminal to M58. SPPL2a and SPPL2b were expressed in human coronary artery endothelial cells (Fig. 9, H and I) and could also be detected in foam as well as endothelial cells in human atherosclerotic lesions by immunohistochemistry (Fig. 9 K). Therefore, we conclude that SPPL2a/b-mediated LOX-1 processing according to the model depicted in Fig. 10 is conserved in humans, strongly supporting a role of these proteases in control of atherosclerosis beyond mice.

Discussion

Our findings identify proteolysis as a major regulatory mechanism of the oxLDL receptor LOX-1. Two pathways, ectodomain shedding and lysosomal degradation, generate LOX-1 NTFs, which induce pro-atherogenic and -fibrotic signaling and require clearance by SPPL2a/b, representing a novel atheroprotective pathway. LOX-1 processing has previously gained interest due to a soluble form of the receptor in plasma (Murase et al., 2000). However, despite its association with vascular and metabolic disorders (Pirillo and Catapano, 2013), its (patho-) physiological function has remained elusive. Different studies based on bovine aortic endothelial cells, macrophages, or HEK cells have suggested serine proteases (Murase et al., 2000), ADAM17 (Zhao et al., 2011), or ADAM10 (Mitsuoka et al., 2009)

to mediate this cleavage. Our data support a predominant function of ADAM10 for liberation of sLOX-1 in HEK and also murine endothelial cells.

In addition to ectodomain shedding, we have identified a so far unknown lysosomal pathway of LOX-1 processing. Based on NTF production, this lysosomal pathway exerts a significantly higher contribution to LOX-1 turnover than ADAM10. Constitutive internalization of LOX-1 has been observed before (Murphy et al., 2008), but not linked to lysosomal proteolysis. Cellular levels of several receptors are controlled by lysosomal degradation, including the EGF receptor (Eden et al., 2009) and many G protein-coupled receptors (Hanyaloglu and von Zastrow, 2008). Usually this involves sorting into intraluminal vesicles by the Endosomal Sorting Complexes Required for Transport pathway (Babst and Odorizzi, 2013). In contrast, LOX-1 processing by lysosomal proteases and SPPL2a/b rather takes place in the limiting membrane of such compartments, thereby releasing the LOX-1 ICD into the cytosol (Fig. 2 A). Whether this cleavage fragment exerts regulatory functions remains to be investigated.

The enhanced pro-atherogenic signaling upon SPPL2a/b inhibition or deficiency was phenocopied by overexpression of the LOX-1 NTF, identifying the accumulation of this fragment as underlying mechanism. The NTF-induced signaling was ligand-independent and also observed in a cell type with no response to oxLDL without overexpression of the full-length receptor. This argues for an autonomous signaling by the LOX-1 NTF. This was driven by MAP kinases, including ERK and p38, in contrast to the ligand induced by the full-length receptor, which also activates NF κ B (Cominacini et al., 2000; Matsunaga et al., 2003). This supports a model of two different LOX-1 signaling modes. With detectable levels of the NTF in aortae from WT mice (Fig. 4 F) and its increase under atherogenic conditions (Fig. S2 A), this novel mode of LOX-1 signaling is likely of pathophysiological importance.

We showed that the TMD of the LOX-1 NTF is critical for its ability to activate MAP kinases, but also for homophilic interactions. Multimerization could be a prerequisite for recruitment of cytosolic proteins or transmembrane signaling adaptors. However, even unbiased immunoprecipitation in combination with mass spectrometry (IP-MS) approaches have so far failed to identify potential candidates. Thus, the direct molecular link between the LOX-1 NTF and the activation of ERK and p38 remains to be identified. Our inhibitor experiments indicated that multiple pathways including MEK1/2, Src family kinases, and ROCK1/2 are involved in this process, suggesting that different protein interactions of the NTF are involved. Whereas an impact of MEK1/2 inhibition on LOX-1 signaling has been described (Hu et al., 2008b; Yang et al., 2017), a role of Src family kinases is a

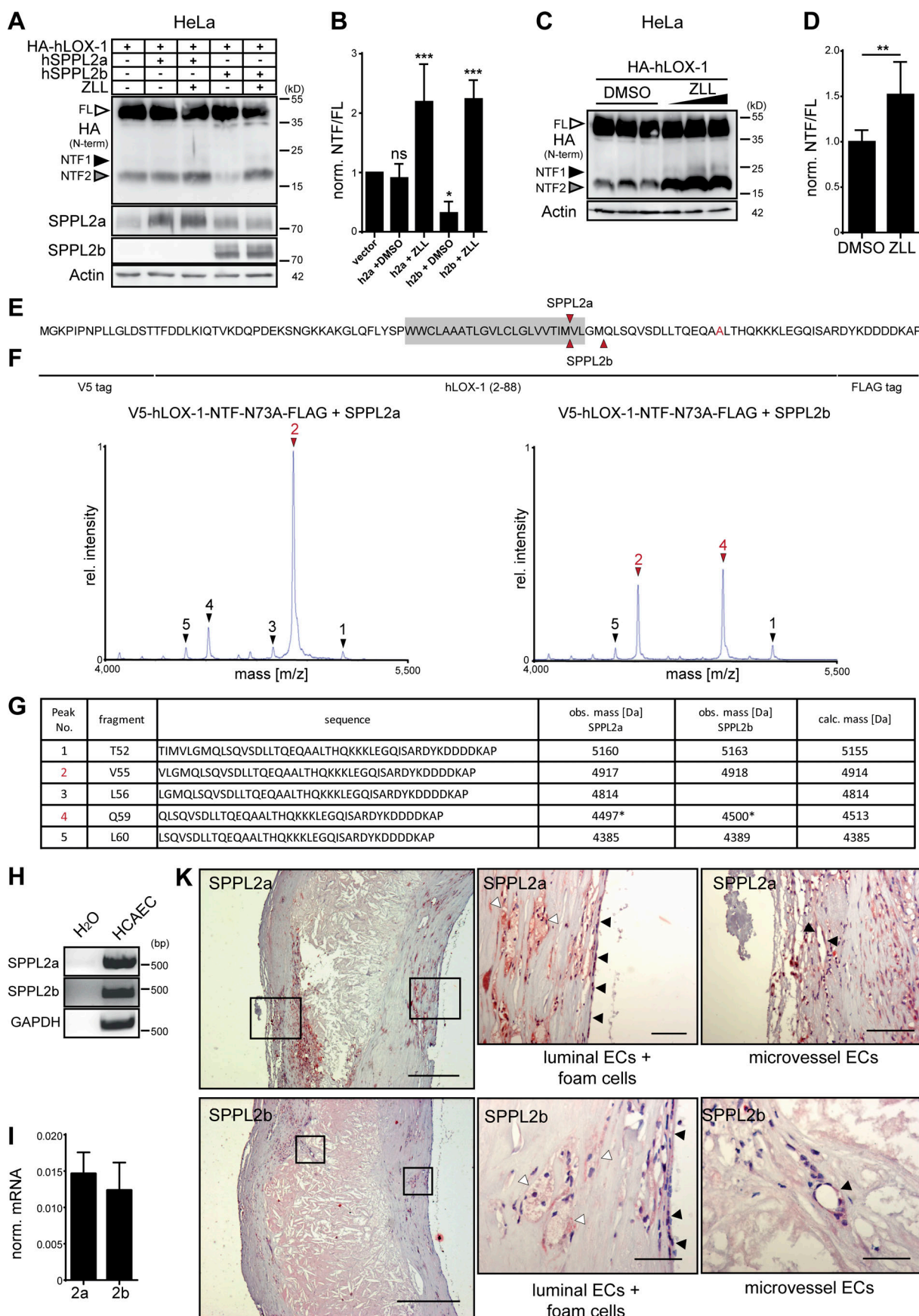


Figure 9. The role of SPPL2a/b for processing of LOX-1 NTFs is conserved in humans. (A) HeLa cells were transfected with HA-tagged hLOX-1 alone or in combination with human SPPL2a (hSPPL2a) or SPPL2b (hSPPL2b-myc). Where indicated, cells were treated with 20 μ M ZLL for 6 h before lysis and Western blot analysis. (B) Quantification of A. $N = 3-4$, $n = 3-4$. One-way ANOVA with Dunnett's post hoc test. (C) Accumulation of hLOX-1 NTFs in HeLa cells upon inhibition of endogenous SPPL2 proteases with 10, 20, and 40 μ M ZLL. (D) Quantification of C for 40 μ M ZLL treatment. $N = 4$, $n = 8$. Student's t test. (E-G) The cleavage sites of human SPPL2a and SPPL2b in the TMD of hLOX-1 were analyzed by MS using V5-hLOX-1 NTF N73A-FLAG as model substrate. Arrows indicate peptides up-regulated by protease overexpression (red, dominant peaks). Peak 4 corresponds to a peptide starting at Q59 with a potential glutamate to pyroglutamate conversion. Rel., relative. (H and I) SPPL2a and SPPL2b are expressed in human coronary artery endothelial cells (HCAECs) as revealed by RT-PCR (H) and qRT-PCR (I). (K) Presence of SPPL2a and SPPL2b in human atherosclerotic plaques was investigated by immunohistochemistry. Bars, 400 μ m; close-ups, 50 μ m. ***, $P \leq 0.001$; **, $P \leq 0.01$; *, $P \leq 0.05$; ns, not significant. N , the number of independent experiments; n , the number of individual samples for quantification. All data are shown as mean \pm SD.

novel observation; however they have been found to be upstream of MAP kinases in other contexts (Singer et al., 2011). As delineated for oxLDL-induced signaling by full-length LOX-1 (Mattaliano et al., 2010), Rho-associated kinases contribute to the pro-atherogenic signaling of the NTF. However, we failed to detect an interaction between the LOX-1 NTF and ROCK-2 (data not shown), which had been reported for full-length LOX-1 (Mattaliano et al., 2010). This indicates that the mechanism activating this pathway differs between full-length LOX-1 and the NTF. In general, links between the ROCK pathway and MAP kinases have been observed (Schwartz, 2004; Zhao et al., 2012; Cui et al., 2014).

Several of the identified LOX-1 NTF downstream targets (Fig. 7 E) have been linked with LOX-1 before, including *Cxcl2* (Mattaliano et al., 2009), *Csf2* (Yang et al., 2017), *Ctgf* (Hu et al., 2009), and *Icam1* (Zhu et al., 2005). These genes cover a wide range of biological functions including endothelial adhesion molecules (*Icam1*), cytokines/chemokines (*Cxcl2*, *Csf2*), and growth factors (*Ctgf*, *Pdgfb*). With regard to atherosclerosis, the up-regulation of these targets triggers multiple axes promoting leukocyte recruitment (Wolpe et al., 1989), immune cell and

smooth muscle cell proliferation (Biwa et al., 2000; Raines, 2004; Zhu et al., 2009), cell migration (Raines, 2004; Al-Alwan et al., 2013), and extracellular matrix deposition (Fan et al., 2000). In particular, the adhesion molecule ICAM-1 plays a critical role in atherosclerotic plaque development (Kitagawa et al., 2002). CTGF is overexpressed in plaques and enhances plaque fibrosis (Cicha et al., 2005). In sum, the effects of increased LOX-NTF levels are not only pro-atherogenic but also pro-fibrotic. This agrees well with a reduced collagen deposition in atherosclerotic lesions of *LOX-1*^{-/-} mice (Hu et al., 2008a). Importantly, the pro-fibrotic activity of LOX-1 is not limited to atherosclerosis, but has also been observed in other disease models (Hu et al., 2009; Lu et al., 2012; Wang et al., 2012; Dai et al., 2014; Deng et al., 2016). It will be of interest if also in these contexts LOX-1 signaling is controlled by SPPL2a/b proteases.

Our findings further establish SPPL2a/b and I-CLIPs as regulators of membrane-associated signaling. This was previously suggested by identifying the CD74 NTF, a substrate of SPPL2a (Schneppenheimer et al., 2013), as a negative regulator of B cell receptor signaling (Hüttel et al., 2015). Further examples are the receptor proteins TREM-2 (Wunderlich et al., 2013; Glebov et al.,

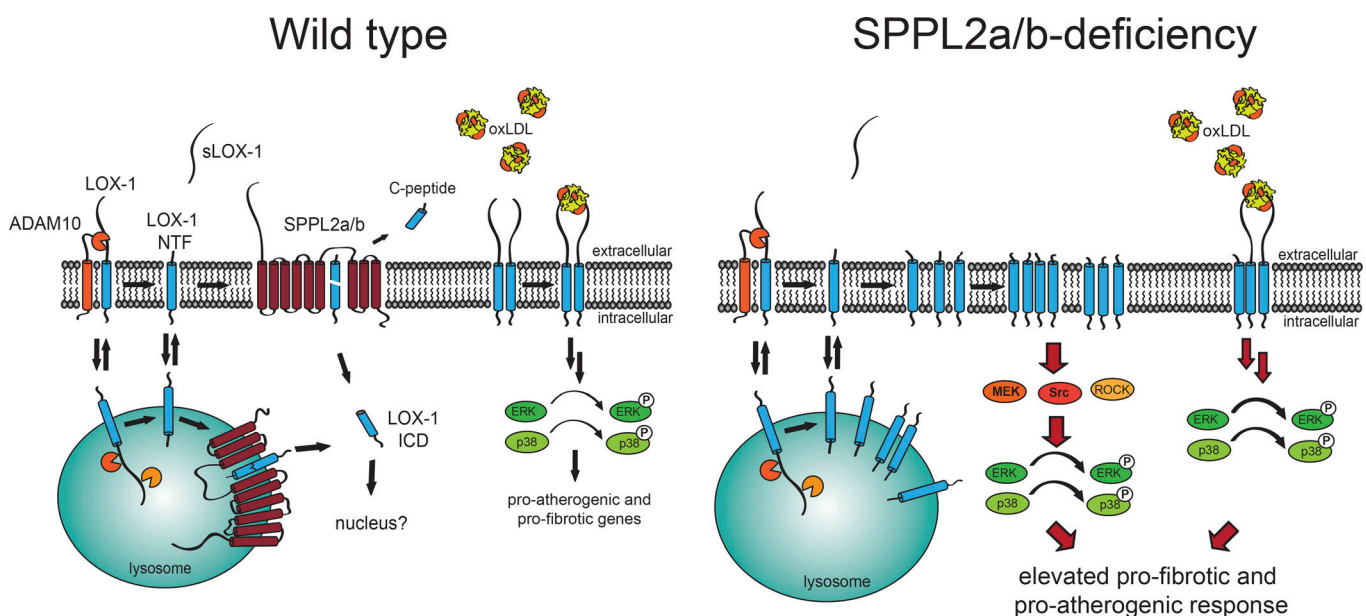


Figure 10. The intramembrane proteases SPPL2a/b control the development of atherosclerosis. SPPL2a and SPPL2b maintain endothelial homeostasis by clearing LOX-1 NTFs generated by ADAM10 and in lysosomes, thereby releasing the LOX-1 ICD. In the absence of SPPL2a/b, LOX-1 NTFs accumulate, enhance oxLDL-induced signaling by full-length LOX-1, and activate MAP kinases in a ligand-independent manner. This promotes endothelial dysfunction and causes a pro-atherogenic and pro-fibrotic phenotype in SPPL2a/b double-deficient mice when challenged with hypercholesterolemia.

2016) and BCMA (Laurent et al., 2015), which are both substrates of γ -secretase. Based on a broad repertoire of type II transmembrane receptors, it may be anticipated that regulation by SPPL2a/b may not be limited to LOX-1.

While proteases like ADAM10 (van der Vorst et al., 2015), ADAM17 (Nicolaou et al., 2017), and γ -secretase (Aoyama et al., 2009) have been implicated in atherosclerosis, this is the first report on the role of SPPL2a/b in this process. Due to poor breeding efficacy of SPPL2a/b double-deficient mice, we applied a novel atherosclerosis model based on overexpression of a gain-of-function variant of murine PCSK9. This protein binds to LDL receptor molecules to induce their lysosomal degradation, thereby mimicking the genetic ablation of the LDL receptor (Bjørklund et al., 2014). PCSK9-transduced mice show all hallmarks of atherosclerosis upon administration of a Western-type diet including hypercholesterolemia, aortic lesion formation, plaque necrosis, and vessel calcification comparable to the more established *Ldlr*^{-/-} or *Apoe*^{-/-} atherosclerosis models (Goettsch et al., 2016; Jacobsen et al., 2017; Rogers et al., 2017; Theodorou et al., 2017). This makes PCSK9 overexpression a valuable tool for the study of atherosclerosis, especially where complex breeding procedures involving multiple alleles would need to be performed. Using this model, we demonstrate that SPPL2a/b exert a relevant impact on atherosclerotic plaques development. Most likely, the performed *in vivo* model underestimates the role of these proteases. First of all, macrophages did not exhibit SPPL2a/b deficiency in our model due to the bone marrow transfer. Though their functionality may be modulated by other substrates like CD74, additional blocking of LOX-1 proteolysis in these cells may further promote atherosclerosis. In addition, the induction of hypercholesterolemia was less efficient in dKO mice as compared with controls. It is quite remarkable that these mice developed larger and more advanced plaques despite 30% lower plasma cholesterol. Presumably, this difference would have been even more pronounced with comparable hypercholesterolemia.

In general, the enhanced MAP kinase signaling, ICAM levels, and fibrosis in plaques of the dKO mice correlate well with our cell-based experiments, where LOX-1 NTF overexpression phenocopies SPPL2a/b inhibition. This strongly suggests impaired LOX-1 proteolysis as the predominant mechanism underlying the *in vivo* phenotype. However, a contribution of low-abundant substrates that have evaded our proteomic analysis is difficult to formally exclude.

Pharmacological inhibition of SPPL2a is currently investigated as a therapeutic approach for immunosuppression based on blocking CD74 cleavage in B cells and dendritic cells. Our results strongly advocate the development of SPPL2a inhibitors, which spare the activity of SPPL2b at least to a relevant degree. Otherwise, they may increase the risk of atherosclerosis by blocking LOX-1 proteolysis. Vice versa, any means of enhancing SPPL2a/b-mediated proteolysis, which would deplete LOX-1 NTFs and thereby abolish their pro-atherogenic effects, may be beneficial to delay the progression of atherosclerosis. If SPPL2a or SPPL2b expression could be induced pharmacologically, this may provide an opportunity to exploit their athero-protective potential.

Materials and methods

Experimental animals

Generation of SPPL2a/b dKO mice has been described previously (Schneppenheim et al., 2014b). All mice were backcrossed for 10 generations in a C57BL/6N Crl background. For all experiments, WT mice with the same genetic background bred and housed in the same animal facility were used as controls. Breeding of mice has been approved by the Ministerium für Energiewende, Landwirtschaft, Umwelt und ländliche Räume of Schleswig-Holstein (V 242.7224.121-3), and animal care and handling were performed in accordance with local and national guidelines. Mice were housed in individually ventilated cages in the animal facility of the Christian-Albrechts-University Kiel, Kiel, Germany. The atherosclerosis experiment was conducted with ethical approval by the Animal Ethics Committee of Maastricht University, Maastricht, Netherlands (permit number 2014-097).

Plasmids

Expression constructs encoding WT murine SPPL2a and SPPL2b fused to a C-terminal myc epitope or their catalytically inactive mutants D416A or D414A as well as corresponding constructs for human SPPL2a were described before (Behnke et al., 2011; Schneppenheim et al., 2013, 2014a,b). C-terminally myc-tagged constructs encoding either WT or catalytically inactive (D421A) human SPPL2b were derived from previously described cDNAs (Fluhrer et al., 2006) and inserted into pcDNA3.1 Hygro+ vectors (Thermo Fisher Scientific) using HindIII and XhoI restriction sites. The open reading frame coding for murine LOX-1 was amplified from a LOX-1 expression plasmid that was a kind gift of Tatsuya Sawamura (National Cerebral and Cardiovascular Center, Osaka, Japan). The PCR product comprising an N-terminally appended HA epitope was ligated into pcDNA3.1 Hygro+ via BamHI and XbaI restriction sites. Based on this plasmid, glycosylation mutants of the murine oxLDL receptor were generated by mutating N72 and N92 to alanines. With the exception of Fig. 9, where human LOX-1 (hLOX-1) and SPPL2a/b (hSPPL2a, hSPPL2b) constructs were employed, in all other experiments the murine cDNAs were used. A GFP-encoding pMSCV puro plasmid was a kind gift of Michael Engelke (University of Göttingen, Göttingen, Germany). Untagged murine full-length LOX-1 or the putative murine LOX-1 NTF consisting of amino acids 1–88 of the receptor was cloned into the pMSCV puro vector (Clontech) using BglII and XhoI restriction sites. Correspondingly, a HA-LOX-1-FLAG construct in this vector was generated. A murine LOX-1 cDNA carrying an N-terminal or C-terminal 3xFLAG-tag was ligated into pcDNA4.0 TO. The coding sequence of hLOX-1 was obtained from Sinobiological, fused to an N-terminal HA tag, and cloned into pcDNA3.1 Hygro(+) via BamHI and XbaI restriction sites. For mass-spectrometric determination of the SPPL2a/b cleavage sites in human and murine LOX-1 NTFs, coding sequences of NTFs comprising amino acids 1–88, with appended N-terminal V5- and C-terminal FLAG epitopes, were inserted into pcDNA3.1 Hygro+. In these constructs, the glycosylated asparagine residues N72 (murine) and N73 (human) were mutated to alanine to reduce complexity of mass spectrometric analysis. HA- or untagged TMD mutants of murine LOX-1 (TMD_{stab}, B1I, B2I, B3I, B3I) as well as the

unphosphorylatable LOX-1 NTF mutant (T2A, S18A, SS30/31AA) were cloned into the pMSCV puro vector using its BglII and XhoI restriction sites.

Cell culture and transfection

HeLa cells (DSMZ), Flip-In T-REx 293 (Invitrogen), HEK293 ADAM10/17 KO cells, MEFs, and Platinum-E retroviral packaging cells (Cell Biolabs, Inc.) were cultivated in DMEM (GIBCO) supplemented with 10% FCS (Biocrom) as well as 100 U/ml penicillin (Sigma-Aldrich) and 100 µg/ml streptomycin (Sigma-Aldrich). ADAM10 and ADAM17 single- and double-deficient HEK293 cells were generated by CRISPR/Cas9 genome editing and initially described in [Riethmueller et al. \(2016\)](#). iMAECs were a kind gift of Prof. Hanjoong Jo (Emory University, Atlanta, GA) and cultured as described in [Bond et al. \(2010\)](#).

MEFs were isolated from 13.5-d-old embryos from WT, *SPPL2a*^{-/-}, *SPPL2b*^{-/-}, and *SPPL2a/b* double-deficient mice. After removing the head and internal organs, embryos were cut into small pieces and incubated in Trypsin-EDTA for 15 min at 37°C. The resulting tissue pieces were dissociated by pipetting and the cell suspension transferred to 12 ml prewarmed DMEM supplemented with 10% FCS and antibiotics. Cells were sedimented, washed once in fresh medium, and plated out for culture. For immortalisation, MEFs were transfected at an early passage with an expression plasmid of the SV40 large T antigen (pMSSVLT; [Schuermann, 1990](#)). After an average of 10 passages, immortalized cells were used for experiments.

Bone marrow-derived dendritic cells (BMDCs) were generated as described in [Schneppenheim et al. \(2014b\)](#) based on the protocol published by [Lutz et al. \(1999\)](#). For detection of N-terminal fragments of TNF, BMDCs were activated for 6 h with 500 ng/ml lipopolysaccharides from *Escherichia coli* (Sigma-Aldrich).

For transient transfection of HeLa, iMAEC, MEF, and Platinum-E cells, Turbofect transfection reagent (Thermo Fisher Scientific) was applied. Flip-In T-REx 293 cells stably expressing murine LOX-1 were generated by transfection with the respective construct and the pOG44 vector encoding the Flp recombinase followed by selection with 100 µg/ml hygromycin and 10 µg/ml blasticidin (both Invivogen). After selection, surviving clones were combined and further analyzed as polyclonal cell lines. To induce transgene expression, 10 µg/ml doxycycline (Sigma-Aldrich) was added to the medium for 24 h. To ensure homogenous expression of the LOX-1 NTF in transiently transfected HEK293 cells, when analysis of signaling pathways was intended, cells were transfected in 6-cm cell culture dishes with 2 µg of either a LOX-1 NTF coding construct or a corresponding empty vector harboring a puromycin resistance cassette (pMSCV). 1 d after transfection, fresh medium containing 10 µg/ml puromycin was added, and cells were incubated for 4 d before further processing for Western blot analysis.

In LOX-1-expressing cell lines, LOX-1-dependent signal transduction was stimulated with 40 µg/ml oxLDL obtained from Hycultec. To influence proteolytic processing of LOX-1, several compounds were added, if not indicated differently, 24 h before analysis to the medium of cultured cells. The lysosomal acidification inhibitor bafilomycin A1 (Sigma-Aldrich) was used in a final concentration of 100 nM. To inhibit cysteine and serine

proteases, E-64d (40 µM; Enzo), Leupeptin (2.5 µM; Roth), and AEBSF (500 µM; Sigma-Aldrich) were applied. The cell-permeable Pepstatin A-methyl ester (10 µM; Merck) was used to interfere with the activity of aspartyl proteases. Activity of the metalloproteinases ADAM10 and ADAM17 was blocked by marimastat (10 µM; Sigma-Aldrich) or stimulated by treatment with ionomycin (1 µM; Sigma-Aldrich) or PMA (100 nM; Sigma-Aldrich), respectively. SPPL2 proteases were inhibited by application of the SPP family inhibitor ZLL (Peptanova) in concentrations ranging from 10 to 40 µM. For kinase inhibition, the MEK1/2-inhibitor U0126 (25 µM; Sigma-Aldrich), the Src-family inhibitor Saracatinib (1 µM; Selleckchem), or the ROCK inhibitor Y-27632 (10 µM; Cayman Chemicals) was applied. To allow for detection of CTGF in lysates of empty vector or LOX-1 NTF-expressing iMAECs, Brefeldin A (Sigma-Aldrich) was applied in a concentration of 1 µg/ml to the culture medium for 6 h before lysis of the cells. Except for Leupeptin, E64-d, and Y-27632, which were applied as aqueous solutions, all small molecule inhibitors were dissolved in DMSO, which was used as solvent control in respective experiments.

Retroviral transduction

For generation of ecotropic retroviruses for transduction of iMAEC and MEF cells, Platinum-E cells were transfected using Turbofect transfection reagent. After 48 h, virus-containing supernatants were removed from Platinum-E cultures and passed through a 20-µm filter (BD Biosciences). Subsequently, supernatants supplemented with 8 µg/ml polybrene (Sigma-Aldrich) were added to the respective cells seeded a day before in 10-cm culture dishes. 1 d after transduction, supernatants were replaced by fresh culture medium containing 10 µg/ml puromycin (Invivogen). Stably transduced cells were maintained as polyclonal cell lines without subcloning.

Protein extraction and Western blot analysis

Cell and tissue lysis was performed as described in [Schneppenheim et al. \(2013\)](#). In brief, cells were harvested by centrifugation and subsequently extracted in lysis buffer (50 mM Tris/HCl, pH 7.4, 150 mM NaCl, 1.0% Triton X-100, and 0.1% SDS) supplemented with Complete protease inhibitor mix (Roche), 0.5 µg/ml Pepstatin A (Sigma-Aldrich), 4 mM EDTA, and 4 mM Pefabloc SC Protease Inhibitor (Roth). Aortic vessels were flushed with PBS and cleaned from adherent adipose and connective tissue. For lysis, 150 µl of lysis buffer and ceramic beads was added to each aorta, which was homogenized by vigorous shaking of the mixture in a Precellys homogenizer (Peqlab). Afterward, cell and tissue suspensions were sonicated using a Branson Sonifier 450 (Emerson Industrial Automation) and incubated at 4°C for 1 h. The remaining debris was pelleted by centrifugation at 13,000 g for 10 min at 4°C, and protein concentrations of supernatants were determined using the Pierce BCA Protein Assay Kit (Thermo Fisher Scientific). After lysis, protein lysates were complemented with the required amount of reducing SDS-PAGE sample buffer according to [Laemmli \(1970\)](#) and denatured for 10 min at 56°C.

For recovery of sLOX-1 from conditioned media of HA-LOX-1-FLAG or mLOX-1-3xFLAG expressing iMAEC or HEK293 cells,

these were cultured in serum free medium for 30 min before stimulation with ionomycin or PMA for 30 min. After stimulation, 800 μ l supernatant was supplemented with 200 μ l 100% (wt/vol) TCA for 1 h at 4°C. Precipitated proteins were sedimented by centrifugation at 13,000 *g* for 10 min at 4°C. The resulting pellet was washed once with ice-cold acetone before resuspension in reducing SDS-PAGE sample buffer and denaturation at 95°C for 10 min.

Electrophoretic separation by SDS-PAGE with a standard Tris-glycine buffer system (Laemmli, 1970), semidry transfer to nitrocellulose membranes, and immunodetection were conducted as described previously (Schröder et al., 2010). Monoclonal antibodies against HA (3F10), myc (9B11), V5, and FLAG (M2) epitope tags were obtained from Roche, Cell Signaling, or Sigma-Aldrich, respectively. sLOX-1 was detected applying a polyclonal goat antibody directed against the C terminus of this protein (AF1564; R&D Systems). To allow detection of LOX-1 NTFs, rabbits were immunized with a synthetic peptide corresponding to the amino acids 2–19 of the protein (Pineda Antikörper Service). Similarly, a polyclonal antiserum against residues 575–592 of human SPPL2b was raised. In both cases, antisera were affinity-purified against the immobilized immunogens before use. Polyclonal antibodies for detection of murine SPPL2a (Behnke et al., 2011), murine SPPL2b (Schneppenheim et al., 2014b), and human SPPL2a (Schneppenheim et al., 2014a) were described before. The polyclonal anti-TNF antibody has been described earlier (Mentrup et al., 2015). Murine CD74 was detected using the In-1 antibody directed against the N terminus of the protein (BD Biosciences). For analysis of signaling pathways, monoclonal antibodies against the phosphorylated forms of ERK1/2 (T202/Y204, D13.14.4E), p38 (T180/182, 3D7), p65 (S536, 93H1), and Akt (S473, D9E) as well as total ERK1/2 (137F5), p38 (D13E1), p65 (C22B4), and Akt (C67E7) from Cell Signaling were used. Phosphorylated and total forms of these kinases and signaling factors were detected from the same membranes. Therefore, immunodetection of the phosphorylated form was performed first. Subsequently, bound antibodies were removed from the membrane by incubation in 100 mM glycine-HCl, 20 mM magnesium acetate, and 50 mM KCl, pH 2.2, for 45 min at 60°C. Membranes were washed several times in 25 mM Tris-HCl, pH 7.4, 137 mM NaCl, 2.7 mM KCl, and 0.1% (vol/vol) Tween-20 (TBS-T), and unspecific binding sites were reblocked for at least 15 min in 5% (wt/vol) dry skim milk powder in TBS-T. Then, primary antibodies against the total forms of the respective kinases were applied, starting a second round of immunodetection for providing a suitable loading control from the same membrane. Murine ICAM-1 was detected with the monoclonal antibody YN1/1.7.4 from BioLegend. CTGF was detected with the polyclonal E-5 antibody from Santa Cruz Biotechnology. Primary antibodies were diluted in 5% milk powder (Roth) dissolved in TBS-T. For detection of phosphorylated proteins, 5% BSA (wt/vol; Roth) in TBS-T was used as antibody diluent. Horseradish peroxidase-conjugated secondary antibodies were purchased from Dianova. Detection of chemiluminescent signals was performed with a LAS4000 imaging system (GE Healthcare) and quantified densitometrically using ImageJ.

Cross-link

HeLa cells were seeded in 6-cm dishes and transfected on the following day as described before. On the next day, cross-linking was performed using bis(sulfosuccinimidyl)suberate (BS³; Thermo Fisher Scientific) as described in Matsunaga et al. (2007) with slight modifications. In brief, cells were washed three times with ice-cold PBS and incubated with 1 mM BS³ in PBS or with PBS alone for 30 min on ice. Next, the cross-linking medium was removed and the remaining BS³ was quenched in 20 mM Tris-HCl, pH 7.4, in PBS for 15 min on ice. Finally, cells were scraped off in 500 μ l PBS complemented with Complete Protease inhibitor mix and processed for Western blot analysis as described above.

oxLDL uptake assays

40,000 iMAECs per well were seeded in black 96-well plates and preincubated for 4 h with either DMSO as control, 100 nM bafilomycin A1, or 10 μ M marimastat. Afterwards, cells were treated with 10 μ g/ml DiI-oxLDL (Thermo Fisher Scientific) for 4 h, washed three times with prewarmed PBS, and analyzed for DiI-fluorescence in a Synergy HT multi-detection reader (BioTek).

Immunoprecipitation (IP)

Cell lysates were prepared in IP buffer (50 mM Tris-HCl, 150 mM NaCl, 1% (wt/vol) Triton X-100, and 4 mM EDTA) supplemented with the same proteinase inhibitors as the standard cell lysis buffer described above. Incubation with primary antibodies was performed at 4°C overnight under continuous end-over-end rotation. The following day, 50 μ l equilibrated Protein G Agarose beads (Thermo Scientific) were added and the incubation continued for 1 h. Beads were recovered by centrifugation, washed five times with IP buffer, and finally eluted by boiling in reducing SDS-PAGE sample buffer.

Indirect immunofluorescence

Immunocytochemical stainings were performed as described previously (Schröder et al., 2010). Cells grown on coverslips were fixed with 4% (wt/vol) paraformaldehyde. Lysosomal compartments were visualized with the 2D5 monoclonal LAMP-2 antibody (Radons et al., 1992). Alexa 488- and 594-conjugated secondary antibodies were purchased from Molecular Probes. Nuclei were stained with DAPI (Sigma-Aldrich), which was included in the embedding medium at a concentration of 1 μ g/ml. Images were acquired with an Olympus FV1000 confocal laser scanning microscope and further processed with Olympus Fluoview software and Adobe Photoshop software.

Flow cytometry

FACS analysis of stably transfected, inhibitor- or TNF (Immunotools)-treated iMAECs was facilitated by an antibody against murine ICAM-1 (YN1/1.7.4) conjugated to the fluorophore APC. For determination of surface LOX-1 levels in receptor overexpressing iMAECs, LOX-1 was first marked with the AF-1564 antibody (R&D Systems) before labeling of the primary antibody with an anti-goat-Alexa 647 conjugate (Molecular Probes). After detachment with Accutase (eBioscience) for

5 min, cells were washed once in FACS buffer (PBS + 2% FCS + 2 mM EDTA) and subsequently stained with the indicated antibodies for 1 h at 4°C. After subsequent additional staining with propidium iodide (BD Biosciences), cells were resuspended in 200 µl FACS buffer and analyzed using a FACS Canto flow cytometer (BD Biosciences) and the FACSDiva software (BD Biosciences). Further data processing was performed with the FlowJo Software (Tree Star).

To assess the reconstitution of B cell development after bone marrow transplantation in the atherosclerosis experiment, cell suspensions were prepared from harvested spleens by passing the tissue through a 70-µm cell strainer (Greiner). Splenocytes were incubated in erythrocyte lysis buffer (150 mM NH₄Cl and 10 mM NaHCO₃, pH 7.4) for 2 min on ice, washed, and filtered through a 70-µm cell strainer. Subsequently, splenic cells were blocked with anti-CD16/32 (clone 93; eBioscience), washed, and stained with antibodies against B220 (RA3-6B2; PE-Cy7; eBioscience), CD21 (8D9; PE; eBioscience), and CD24 (30-F1; APC; eBioscience). Cells were analyzed using a FACS Canto II flow cytometer (BD Biosciences) and FACSDiva software v6 (BD Biosciences) for data interpretation.

For quantification of LOX-1 internalization, iMAECs stably overexpressing LOX-1 were incubated for 30 min on ice with an antibody against the C terminus of the protein in the presence of 10 µM marimastat or DMSO as control. Cells were washed twice with ice-cold PBS and subsequently chased for 2 h at 37°C. After detachment of the cells from the culture dishes, remaining surface LOX-1 was labeled with an anti-goat-Alexa 647 antibody and detected using a FACS Canto cytometer as described above.

Cleavage site determination

Epitope-tagged LOX-1 NTFs (V5-LOX-1-NTF-N72A-FLAG, V5-hLOX-1-NTF-N73A-FLAG) were transiently expressed in T-REx 293 cells with or without stable overexpression of SPPL2a or SPPL2b. The C-peptides released by the SPPL2-mediated intramembrane cleavage were recovered from conditioned media using anti-FLAG M2-conjugated agarose beads (Sigma-Aldrich). After repeated washing with IP-MS buffer (0.1% *n*-octyl glucoside, 10 mM Tris/HCl, pH 8.0, 5 mM EDTA, and 140 mM NaCl) and sterile water, peptides were eluted using a trifluoroacetic acid/acetonitrile/water mixture (1:20:20, vol/vol/vol) saturated with α -cyano-4-hydroxycinnamic acid. The dissolved samples were dried on a stainless plate and subjected to Matrix-assisted laser desorption ionization-time of flight (MALDI-TOF)-MS analysis using a VoyagerDE STR instrument (Applied Biosystems).

Proteomic analysis of murine aorta

The total proteome of three biologically independent aortic samples from WT and SPPL2a/b-deficient mice was analyzed and quantitatively compared. Each sample was prepared from pooled aortae of two age- and sex-matched mice of the respective genotype, which were extracted in 150 µl lysis buffer. Lysate corresponding to 150 µg protein was mixed with 100 µl 30% acrylamide, 1.25 µl TEMED (N,N,N',N'-tetramethylethylenediamine) and 5 µl of 10% ammonium persulfate to trap proteins in a gel matrix, fixed (50% methanol and 10% acetic acid), washed with water, and cut into pieces. After dehydration,

proteins were reduced with 10 mM dithiothreitol at 60°C for 30 min and alkylated using 55 mM iodoacetamide. Subsequently, proteins were digested by adding 200 µl of trypsin solution (10 ng/µl) in 50 mM ammonium bicarbonate (Shevchenko et al., 2006). After extraction using 10% formic acid and 50% and 100% acetonitrile, peptides were purified using the C18 SepPak column system (Waters) and lyophilized.

Peptides were then labeled using TMT 6plex (Thermo Fisher Scientific) according to the manufacturer. Samples were named WT pool #1 (TMT126), WT pool #2 (TMT128), WT pool #3 (TMT130), dKO pool #1 (TMT127), dKO pool #2 (TMT129), and dKO pool #3 (TMT131) and purified using the C18 SepPak column system. Then, peptides were combined and fractionated by high pH reversed-phase chromatography on a Phenomenex Gemini 3u C18 110A 250 × 3 mm column using a Dionex Ultimate 3000 HPLC as described (Treitz et al., 2015), reconstituted in 20 µl 5% formic acid and submitted to liquid chromatography-tandem MS analysis, which was performed using a Dionex U3000 nanoUHPLC coupled to a Q Exactive Plus mass spectrometer (both from Thermo Scientific). 8 µl of each fraction was loaded on a trap column (10 mm × 300 µm; 3 µm; 100 Å; Acclaim Pepmap 100 C18; Dionex), and separation was performed using an Acclaim PepMap 100 C18 analytical column (50 cm × 75 µm; 2 µm; 100 Å; Dionex) with a flow-rate of 300 nl/min using a 180-min gradient. MS data were acquired from 5 to 145 min with MS full scans between 300 and 1,800 (*m/z*) at a resolution of 70,000 at *m/z* 200. The 15 most intense precursors were subjected to high-energy collisional fragmentation. MS data were searched using the SequestHT algorithm in Proteome Discoverer 2.2 (Thermo Scientific) against the entire reviewed Ensembl protein database of *Mus musculus* (v. 6.7.2017) with full enzyme specificity. Static modifications were carbamidomethylation on cysteine residues, TMT on lysines and peptide N termini, while oxidation of methionine residues was set as dynamic modification. Two missed cleavages were allowed. Search tolerances were set to 10 ppm for MS and 0.02 Dalton for MS/MS. The protein group identifications were further filtered based on a false discovery rate (FDR) confidence ≤ 0.01. TMT reporter ion ratio quantification (Proteome Discoverer 2.2) was reported for three independent biological replicates (WT/dKO). Reporter ion abundances for the six channels were used to perform a two-tailed *t* test, and analysis of the local FDR showed that a *t* test *P* value of 0.04 corresponded to a FDR of 5%, hereby determining our significance cut-off for reproducibility of differential protein abundance. Boundaries for differential abundances between WT and dKO were set to statistically significant fold changes of more than 1.4 (Table S2).

RT-PCR and quantitative gene expression analysis

Total cellular RNA was isolated with the NucleospinRNA Kit (Macherey Nagel) according to the manufacturer's recommendations. Subsequently, RNA was transcribed into cDNA using the RevertAid First Strand cDNA Synthesis Kit (Thermo Scientific). RT-PCR analysis of human SPPL2 protease expression was performed with the following primers: hSPPL2a-RT-fw: 5'-AGTTGCCCAACTTCAAGTCATG-3', hSPPL2a-RT-rv: 5'-CCA AATGGTCCATCATCTGATAG-3', hSPPL2b-RT-fw: 5'-ATCTTC

ACGCGTTTCGGCCGCA-3', hSPPL2b-RT-rv: 5'-CCAGGCCCACTG GTCCTCGTTG-3', hGAPDH-RT-fw: 5'-AGGTCCGAGTCAACGGAT TTG-3', hGAPDH-RT-rv: 5'-GTGATGGCATGGACTGTGGT-3'. To analyze potential differences in the expression of atherosclerosis-related genes due to overexpression of the putative LOX-1 NTF, mouse endothelial cell biology and mouse atherosclerosis RT² Profiler PCR arrays (Qiagen) were employed using 500 ng of total RNA isolates obtained from two independently generated iMAEC lines stably transduced either with an untagged LOX-1 1-88 (NTF) coding construct or a corresponding empty vector control. Arrays were performed in a 384-well format according to the manufacturer's recommendations. dCt-values were compared between the four lines, and candidate genes were selected based on an increased or decreased mean NTF/empty vector ratio and low variability between the individual lines per construct. Genes with highly different expression in equally transduced lines were excluded for further follow-up.

For quantitative PCR (qPCR), 0.5 µl cDNA was analyzed using the Universal Probe Library System (Roche) and a Light Cycler 480II (Roche) as described in Mentrup et al. (2015). The following primers were used: mCtgf (probe 71) fw: 5'-TGACCTGGA GGAAACATTAAGA-3'; mCtgf (probe 71) rev: 5'-AGCCCTGTA TGTCTTCACACTG-3'; mIcam1 fw (probe 64): 5'-GCTACCATC ACCGTGTACTTCG-3'; mIcam1 rev (probe 64): 5'-TGAGGTCTT TGCCTACTTGC-3'; mPdgfb fw (probe 74): 5'-CGAGGGAGGAGG AGCCTA-3'; mPdgfb rev (probe 74): 5'-GTCTTGCCTCGGCG ATTA-3'; mCxcl2 fw (probe 26): 5'-AAAATCATCCAAAAGATA CTGAACAA-3'; mCxcl2 rev (probe 26): 5'-CTTTGGTTCTTCGGT TGAGG-3'; mCcl5 fw (probe 110): 5'-TGCAGAGGACTCTGAGAC AGC-3'; mCcl5 rev (probe 110): 5'-GAGTGGTGTCCGAGCCATA-3'; mKdr fw (probe 18): 5'-CCCCAAATTCATTATGACAA-3'; mKdr rev (probe 18): 5'-CGGCTCTTTCGCTTACTGTT-3'; mPdgfrb fw (probe 67): 5'-TCAAGCTGCAGGTCAATGTC-3'; mPdgfrb rev (probe 67): 5'-CCATTGGCAGGGTGAATC-3'; mP4 fw (probe 64): 5'-TCTGGGATCCATCTTAAGCAC-3'; mP4 rev (probe 64): 5'-CCATTCTTCAGGGTGGCTAT-3'; mCs2 fw (probe 79): 5'-GCATGTAGAGGCCATCAAAGA-3'; mCs2 rev (probe 79): 5'-CGGGTCTGCACACATGTTA-3'; mFgf1 fw (probe 41): 5'-CAG CCTGCCAGTTCTTCAG-3'; mFgf1 rev (probe 41): 5'-GGCTGC GAAGGTTGTGAT-3'; mCol3a1 fw (probe 49): 5'-TCCCTGGA ATCTGTGAATC-3'; mCol3a1 rev (probe 49): 5'-TGAGTCGAA TTGGGGAGAAT-3'; mCflar fw (probe 51): 5'-GCAGAAGCTCTC CCAGCA-3'; mCflar rev (probe 51): 5'-TTTGTCCATGAGTTCAAC GTG-3'. Expression of individual genes was normalized to that of Tubal1, which was detected using the following primers: mTubal1 fw (probe 88): 5'-CTGGAACCCACGGTCATC-3'; mTubal1 rev (probe 88): 5'-TGAGTGGCCACGAGCATAG-3'.

Bone marrow transplantation and atherosclerosis model

1 wk before bone marrow transplantation, female WT and SPPL2a/b dKO mice received water supplemented with antibiotics (neomycin, 100 mg/liter, and Polymyxin B sulfate, 60,000 U/liter, both from Gibco), which was continued for 5 wk after the procedure. Mice were exposed to 6 Gy total body irradiation 1 d before and on the day of transplantation with 5×10^6 bone marrow cells isolated from WT mice. After a recovery period of 5 wk, hypercholesterolemia was induced by

adeno-associated viral expression of a gain-of-function mutant of PCSK9 (rAAV8-D377Y-mPCSK9) according to Bjørklund et al. (2014). Viral particles produced by the University of North Carolina Vector Core were injected into the tail vein of the mice (10^{11} genome copies). Concurrently, mice were fed an HCD containing 0.25% cholesterol in addition to 15% cacao butter, 1% corn oil, 40.5% sucrose, 10% corn starch, and 5.95% cellulose (824171; Special Diets Services) for 9 wk. Plasma concentrations of triglycerides and cholesterol were determined at baseline just before HCD initiation as well as after 9 wk using standard enzymatic kits (Cholesterol FS'10; Triglycerides FS 5' Ecoline; Diagnostic Systems GmbH) according to the manufacturer's instructions. Prior to blood sampling from the tail vein, mice were fasted for 4 h.

Female LDL receptor-deficient (*Ldlr*^{-/-}) mice ($n = 4$, C57Bl6 background) were obtained from in-house breeding, irradiated 2× with 6 Gy, and reconstituted with WT bone marrow, followed by HCD (824171; Special Diets Services) feeding for 3 wk (permit number 2014-019; Maastricht University, Netherlands).

Histological analysis

After 9 wk of HCD feeding, mice were anesthetized, euthanized, and perfused with PBS containing nitroprusside (0.1 mg/ml; Sigma-Aldrich). Hearts were excized and fixed in 1% paraformaldehyde overnight. Serial paraffin sections of the aortic root were cut (4 µm) and stained with H&E (Sigma-Aldrich) for morphometric analysis of plaque size and necrotic core area (defined as acellular region). Total plaque areas per mouse were obtained by averaging measurements of five consecutive H&E-stained sections (4 µm, 20 µm apart) at the same anatomical location in the aortic root, starting at the first appearance of the medial layer. Plaque stages were determined as previously described (Gijbels et al., 1999), with slight modifications. Plaques were classified as early (foam cell-rich but lacking a necrotic core), moderately advanced (containing a fibrotic cap and often a necrotic core, but no medial macrophage infiltration), and advanced lesions (typified by medial macrophage infiltrates, elastic lamina degradation, and more pronounced necrosis and fibrosis). Atherosclerotic lesions were further analyzed for abundance of macrophages (1:200; MAC3; clone M3/84; BD Biosciences), smooth muscle cells (1:3,000; αSMA; clone 1A4; Sigma-Aldrich) and collagen content (Sirius Red; Polysciences). Sections (MAC3, αSMA) were subjected to heat-induced antigen retrieval using citrate buffer (pH 6; DAKO), and specific antigen-antibody binding was visualized using appropriate biotinylated secondary antibodies, ABC horseradish peroxidase (Vector Laboratories), and DAB substrate kit (DAKO). Cell nuclei were counterstained with hematoxylin. Pictures were taken using a Leica DM3000 light microscope, and sections were analyzed in a blinded manner using Adobe Photoshop CS6 software.

Immunohistochemistry of human plaque sections

Collection, storage, and use of human carotid artery tissue in the Maastricht Pathology Tissue Collection and patient data confidentiality were performed after informed consent and in agreement with the "Code for Proper Secondary Use of Human Tissue in the Netherlands," which is in accordance with the

guidelines of and approved by the medical and ethical committee of Maastricht University Medical Centre, Maastricht, Netherlands. Human carotid endarterectomy segments were fixed in paraformaldehyde and paraffin-embedded. Sections were incubated with polyclonal antisera against human SPPL2a or SPPL2b (described above), followed by detection with Brightvision secondary antibodies (Immunologic) and Vector Red (Vector Laboratories). Cell nuclei were counterstained with hematoxylin. Pictures were taken using a Leica DM3000 light microscope.

Statistical analysis

For statistical analysis, an unpaired Student's *t* test or a one-way ANOVA with either Tukey's or Dunnett's post hoc testing was performed as indicated in the individual figure legends using GraphPad Prism. All data are shown as mean \pm SD. Where stably transduced iMAECs were used, data quantification is based on at least three independently generated cell lines. *N* describes the number of independent experiments, and *n* depicts the number of individual samples for quantification.

Online supplemental material

Fig. S1 summarizes supporting data from the analysis of LOX-1 NTF generation and the mass-spectrometric cleavage site determination. Fig. S2 depicts the increase of LOX-1 NTFs upon induction of atherosclerosis as well as the reconstitution of the B cell defect of SPPL2a/b-deficient mice by bone marrow transplantation. In Fig. S3, data addressing the potential involvement of other SPPL2a/b substrates are shown. Table S1 shows the full dataset obtained from the performed mouse endothelial cell biology and mouse atherosclerosis RT² Profiler PCR arrays. In Table S2, all proteins identified in the comparative proteomic analysis of WT and SPPL2a/b-deficient aortae are listed.

Acknowledgments

We thank Sebastian Held, Marlies Rusch, and Martina Haug-Kröper for excellent technical assistance. We are grateful to Tatsuya Sawamura (National Cerebral and Cardiovascular Center, Osaka, Japan), Michael Engelke (University of Göttingen, Göttingen, Germany), and Hanjoong Jo (Emory University, Atlanta, GA) for plasmids and cell lines. We thank Kristiaan Wouters (Maastricht University, Maastricht, Netherlands) for providing material from LDL receptor-deficient mice. We are also grateful for support by the Z3 imaging unit of the SFB877.

This work was supported by the Deutsche Forschungsgemeinschaft as part of the SFB877 (project B7 to B. Schröder, and project Z2 to A.O. Helbig and A. Tholey), and the research group FOR2290 (projects FL 635/3-1 to R. Flührer, and STE847/4-1 to H. Steiner), as well as grants SCHR 1284/1-1 and SCHR1284/2-1 (to B. Schröder) and FL 635/2-1 (to R. Flührer). M. Donners and K. Theodorou were supported by the the Netherlands Heart Foundation (Dr. E. Dekker grant 2012T079).

The authors declare no competing financial interests.

Author contributions: T. Mentrup, K. Theodorou, F. Cabrera-Cabrera, A.O. Helbig, K. Happ, M. Gijbels, A.-C. Gradtke, and A. Fukumori performed the experiments and analyzed data.

R. Flührer, A. Fukumori, and H. Steiner conducted the cleavage site determination. A.O. Helbig and A. Tholey contributed the proteomic analysis of aortic samples. B. Rabe provided reagents and protocols including technical advice. K. Theodorou and M. Donners performed the atherosclerosis experiments and contributed to the overall design of the study. T. Mentrup analyzed and interpreted data. B. Schröder designed, conceptualized, and supervised the research. B. Schröder and T. Mentrup wrote the manuscript. All authors contributed to the manuscript editing.

Submitted: 9 August 2017

Revised: 21 August 2018

Accepted: 17 October 2018

References

- Akhmedov, A., I. Rozenberg, F. Paneni, G.G. Camici, Y. Shi, C. Doerries, A. Sledzinska, P. Mocharlar, A. Breitenstein, C. Lohmann, et al. 2014. Endothelial overexpression of LOX-1 increases plaque formation and promotes atherosclerosis in vivo. *Eur. Heart J.* 35:2839–2848. <https://doi.org/10.1093/eurheartj/ehu532>
- Al-Alwan, L.A., Y. Chang, A. Mogas, A.J. Halayko, C.J. Baglione, J.G. Martin, S. Rousseau, D.H. Eidelman, and Q. Hamid. 2013. Differential roles of CXCL2 and CXCL3 and their receptors in regulating normal and asthmatic airway smooth muscle cell migration. *J. Immunol.* 191:2731–2741. <https://doi.org/10.4049/jimmunol.1203421>
- Aoyama, T., K. Takeshita, R. Kikuchi, K. Yamamoto, X.W. Cheng, J.K. Liao, and T. Murohara. 2009. gamma-Secretase inhibitor reduces diet-induced atherosclerosis in apolipoprotein E-deficient mice. *Biochem. Biophys. Res. Commun.* 383:216–221. <https://doi.org/10.1016/j.bbrc.2009.03.154>
- Babst, M., and G. Odorizzi. 2013. The balance of protein expression and degradation: an ESCRT's point of view. *Curr. Opin. Cell Biol.* 25:489–494. <https://doi.org/10.1016/j.ccb.2013.05.003>
- Behnke, J., J. Schneppenheim, F. Koch-Nolte, F. Haag, P. Saftig, and B. Schröder. 2011. Signal-peptide-peptidase-like 2a (SPPL2a) is targeted to lysosomes/late endosomes by a tyrosine motif in its C-terminal tail. *FEBS Lett.* 585:2951–2957. <https://doi.org/10.1016/j.febslet.2011.08.043>
- Beisner, D.R., P. Langerak, A.E. Parker, C. Dahlberg, F.J. Otero, S.E. Sutton, L. Poirot, W. Barnes, M.A. Young, S. Niessen, et al. 2013. The intramembrane protease Sppl2a is required for B cell and DC development and survival via cleavage of the invariant chain. *J. Exp. Med.* 210:23–30. <https://doi.org/10.1084/jem.20121072>
- Bergmann, H., M. Yabas, A. Short, L. Miosge, N. Barthel, C.E. Teh, C.M. Roots, K.R. Bull, Y. Jeelall, K. Horikawa, et al. 2013. B cell survival, surface BCR and BAFFR expression, CD74 metabolism, and CD8- dendritic cells require the intramembrane endopeptidase SPPL2A. *J. Exp. Med.* 210:31–40. <https://doi.org/10.1084/jem.20121076>
- Biwa, T., M. Sakai, M. Shichiri, and S. Horiuchi. 2000. Granulocyte/macrophage colony-stimulating factor plays an essential role in oxidized low density lipoprotein-induced macrophage proliferation. *J. Atheroscler. Thromb.* 7:14–20. <https://doi.org/10.5551/jat1994.7.14>
- Bjørklund, M.M., A.K. Hollensen, M.K. Hagensen, F. Dagnaes-Hansen, C. Christoffersen, J.G. Mikkelsen, and J.F. Bentzon. 2014. Induction of atherosclerosis in mice and hamsters without germline genetic engineering. *Circ. Res.* 114:1684–1689. <https://doi.org/10.1161/CIRCRESAHA.114.302937>
- Bond, A.R., C.W. Ni, H. Jo, and P.D. Weinberg. 2010. Intimal cushions and endothelial nuclear elongation around mouse aortic branches and their spatial correspondence with patterns of lipid deposition. *Am. J. Physiol. Heart Circ. Physiol.* 298:H536–H544. <https://doi.org/10.1152/ajpheart.00917.2009>
- Chen, K., J. Chen, Y. Liu, J. Xie, D. Li, T. Sawamura, P.L. Hermonat, and J.L. Mehta. 2005. Adhesion molecule expression in fibroblasts: alteration in fibroblast biology after transfection with LOX-1 plasmids. *Hypertension.* 46:622–627. <https://doi.org/10.1161/01.HYP.0000179045.95915.b0>
- Cicha, I., A. Yilmaz, M. Klein, D. Raithel, D.R. Brigstock, W.G. Daniel, M. Goppelt-Strube, and C.D. Garlich. 2005. Connective tissue growth factor is overexpressed in complicated atherosclerotic plaques and

- induces mononuclear cell chemotaxis in vitro. *Arterioscler. Thromb. Vasc. Biol.* 25:1008–1013. <https://doi.org/10.1161/01.ATV.0000162173.27682.7b>
- Cominacini, L., A.F. Pasini, U. Garbin, A. Davoli, M.L. Tosetti, M. Campagnola, A. Rigoni, A.M. Pastorino, V. Lo Cascio, and T. Sawamura. 2000. Oxidized low density lipoprotein (ox-LDL) binding to ox-LDL receptor-1 in endothelial cells induces the activation of NF-kappaB through an increased production of intracellular reactive oxygen species. *J. Biol. Chem.* 275:12633–12638. <https://doi.org/10.1074/jbc.275.17.12633>
- Cui, Y., Y.W. Sun, H.S. Lin, W.M. Su, Y. Fang, Y. Zhao, X.Q. Wei, Y.H. Qin, K. Kohama, and Y. Gao. 2014. Platelet-derived growth factor-BB induces matrix metalloproteinase-2 expression and rat vascular smooth muscle cell migration via ROCK and ERK/p38 MAPK pathways. *Mol. Cell. Biochem.* 393:255–263. <https://doi.org/10.1007/s11010-014-2068-5>
- Dai, Y., P. Palade, X. Wang, F. Mercanti, Z. Ding, D. Dai, and J.L. Mehta. 2014. High fat diet causes renal fibrosis in LDLr-null mice through MAPK-NF-kB pathway mediated by Ox-LDL. *J. Cardiovasc. Pharmacol.* 63:158–166. <https://doi.org/10.1097/FJC.0000000000000035>
- Deng, S., T. Jin, L. Zhang, H. Bu, and P. Zhang. 2016. Mechanism of tacrolimus-induced chronic renal fibrosis following transplantation is regulated by ox-LDL and its receptor, LOX-1. *Mol. Med. Rep.* 14: 4124–4134. <https://doi.org/10.3892/mmr.2016.5735>
- De Strooper, B., W. Annaert, P. Cupers, P. Saftig, K. Craessaerts, J.S. Mumm, E.H. Schroeter, V. Schrijvers, M.S. Wolfe, W.J. Ray, et al. 1999. A presenilin-1-dependent gamma-secretase-like protease mediates release of Notch intracellular domain. *Nature*. 398:518–522. <https://doi.org/10.1038/19083>
- Di Pietro, N., G. Formoso, and A. Pandolfi. 2016. Physiology and pathophysiology of oxLDL uptake by vascular wall cells in atherosclerosis. *Vascul. Pharmacol.* 84:1–7. <https://doi.org/10.1016/j.vph.2016.05.013>
- Eden, E.R., I.J. White, and C.E. Futter. 2009. Down-regulation of epidermal growth factor receptor signalling within multivesicular bodies. *Biochem. Soc. Trans.* 37:173–177. <https://doi.org/10.1042/BST0370173>
- Fan, W.H., M. Pech, and M.J. Karnovsky. 2000. Connective tissue growth factor (CTGF) stimulates vascular smooth muscle cell growth and migration in vitro. *Eur. J. Cell Biol.* 79:915–923. <https://doi.org/10.1078/0171-9335-00122>
- Fluhrer, R., G. Grammer, L. Israel, M.M. Condron, C. Haffner, E. Friedmann, C. Böhland, A. Imhof, B. Martoglio, D.B. Teplow, and C. Haass. 2006. A gamma-secretase-like intramembrane cleavage of TNFalpha by the GxGD aspartyl protease SPPL2b. *Nat. Cell Biol.* 8:894–896. <https://doi.org/10.1038/ncb1450>
- Friedmann, E., E. Hauben, K. Maylandt, S. Schleeger, S. Vreugde, S.F. Lichtenthaler, P.H. Kuhn, D. Stauffer, G. Rovelli, and B. Martoglio. 2006. SPPL2a and SPPL2b promote intramembrane proteolysis of TNFalpha in activated dendritic cells to trigger IL-12 production. *Nat. Cell Biol.* 8:843–848. <https://doi.org/10.1038/ncb1440>
- Gijbels, M.J., M. van der Cammen, L.J. van der Laan, J.J. Emeis, L.M. Havekes, M.H. Hofker, and G. Kraal. 1999. Progression and regression of atherosclerosis in APOE3-Leiden transgenic mice: an immunohistochemical study. *Atherosclerosis*. 143:15–25. [https://doi.org/10.1016/S0021-9150\(98\)00263-9](https://doi.org/10.1016/S0021-9150(98)00263-9)
- Gimbrone, M.A. Jr., and G. García-Cardena. 2016. Endothelial Cell Dysfunction and the Pathobiology of Atherosclerosis. *Circ. Res.* 118:620–636. <https://doi.org/10.1161/CIRCRESAHA.115.306301>
- Glebov, K., P. Wunderlich, I. Karaca, and J. Walter. 2016. Functional involvement of gamma-secretase in signaling of the triggering receptor expressed on myeloid cells-2 (TREM2). *J. Neuroinflammation*. 13:17. <https://doi.org/10.1186/s12974-016-0479-9>
- Goettsch, C., J.D. Hutcheson, S. Hagita, M.A. Rogers, M.D. Creager, T. Pham, J. Choi, A.K. Mlynarchik, B. Pieper, M. Kjolby, et al. 2016. A single injection of gain-of-function mutant PCSK9 adeno-associated virus vector induces cardiovascular calcification in mice with no genetic modification. *Atherosclerosis*. 251:109–118. <https://doi.org/10.1016/j.atherosclerosis.2016.06.011>
- Hanyaloglu, A.C., and M. von Zastrow. 2008. Regulation of GPCRs by endocytic membrane trafficking and its potential implications. *Annu. Rev. Pharmacol. Toxicol.* 48:537–568. <https://doi.org/10.1146/annurev.pharmtox.48.113006.094830>
- Hayashida, K., N. Kume, T. Murase, M. Minami, D. Nakagawa, T. Inada, M. Tanaka, A. Ueda, G. Kominami, H. Kambara, et al. 2005. Serum soluble lectin-like oxidized low-density lipoprotein receptor-1 levels are elevated in acute coronary syndrome: a novel marker for early diagnosis. *Circulation*. 112:812–818. <https://doi.org/10.1161/CIRCULATIONAHA.104.468397>
- Herrington, W., B. Lacey, P. Sherliker, J. Armitage, and S. Lewington. 2016. Epidemiology of Atherosclerosis and the Potential to Reduce the Global Burden of Atherothrombotic Disease. *Circ. Res.* 118:535–546. <https://doi.org/10.1161/CIRCRESAHA.115.307611>
- Hu, C., A. Dandapat, L. Sun, J. Chen, M.R. Marwali, F. Romeo, T. Sawamura, and J.L. Mehta. 2008a. LOX-1 deletion decreases collagen accumulation in atherosclerotic plaque in low-density lipoprotein receptor knockout mice fed a high-cholesterol diet. *Cardiovasc. Res.* 79:287–293. <https://doi.org/10.1093/cvr/cvn110>
- Hu, C., A. Dandapat, L. Sun, J.A. Khan, Y. Liu, P.L. Hermonat, and J.L. Mehta. 2008b. Regulation of TGFbeta1-mediated collagen formation by LOX-1: studies based on forced overexpression of TGFbeta1 in wild-type and lox-1 knock-out mouse cardiac fibroblasts. *J. Biol. Chem.* 283:10226–10231. <https://doi.org/10.1074/jbc.M708820200>
- Hu, C., B.Y. Kang, J. Megyesi, G.P. Kaushal, R.L. Safirstein, and J.L. Mehta. 2009. Deletion of LOX-1 attenuates renal injury following angiotensin II infusion. *Kidney Int.* 76:521–527. <https://doi.org/10.1038/ki.2009.234>
- Hüttel, S., K. Kläsener, M. Schweizer, J. Schneppenheim, H.H. Oberg, D. Kabelitz, M. Reth, P. Saftig, and B. Schröder. 2015. Processing of CD74 by the Intramembrane Protease SPPL2a Is Critical for B Cell Receptor Signaling in Transitional B Cells. *J. Immunol.* 195:1548–1563. <https://doi.org/10.4049/jimmunol.1403171>
- Inoue, K., Y. Arai, H. Kurihara, T. Kita, and T. Sawamura. 2005. Overexpression of lectin-like oxidized low-density lipoprotein receptor-1 induces intramyocardial vasculopathy in apolipoprotein E-null mice. *Circ. Res.* 97:176–184. <https://doi.org/10.1161/01.RES.0000174286.73200.d4>
- Jacobsen, K., M.B. Lund, J. Shim, S. Gunneren, E.M. Füchtbauer, M. Kjolby, L. Carramolino, and J.F. Bentzon. 2017. Diverse cellular architecture of atherosclerotic plaque derives from clonal expansion of a few medial SMCs. *JCI Insight*. 2:e95890. <https://doi.org/10.1172/jci.insight.95890>
- Kataoka, H., N. Kume, S. Miyamoto, M. Minami, H. Moriwaki, T. Murase, T. Sawamura, T. Masaki, N. Hashimoto, and T. Kita. 1999. Expression of lectinlike oxidized low-density lipoprotein receptor-1 in human atherosclerotic lesions. *Circulation*. 99:3110–3117. <https://doi.org/10.1161/01.CIR.99.24.3110>
- Kitagawa, K., M. Matsumoto, T. Sasaki, H. Hashimoto, K. Kuwabara, T. Ohtsuki, and M. Hori. 2002. Involvement of ICAM-1 in the progression of atherosclerosis in APOE-knockout mice. *Atherosclerosis*. 160:305–310. [https://doi.org/10.1016/S0021-9150\(01\)00587-1](https://doi.org/10.1016/S0021-9150(01)00587-1)
- Laemmli, U.K. 1970. Cleavage of structural proteins during the assembly of the head of bacteriophage T4. *Nature*. 227:680–685. <https://doi.org/10.1038/227680a0>
- Langosch, D., C. Scharnagl, H. Steiner, and M.K. Lemberg. 2015. Understanding intramembrane proteolysis: from protein dynamics to reaction kinetics. *Trends Biochem. Sci.* 40:318–327. <https://doi.org/10.1016/j.tibs.2015.04.001>
- Laurent, S.A., F.S. Hoffmann, P.H. Kuhn, Q. Cheng, Y. Chu, M. Schmidt-Supprian, S.M. Hauck, E. Schuh, M. Krumbholz, H. Rübsamen, et al. 2015. gamma-Secretase directly sheds the survival receptor BCMA from plasma cells. *Nat. Commun.* 6:7333. <https://doi.org/10.1038/ncomms8333>
- Li, D., and J.L. Mehta. 2000. Antisense to LOX-1 inhibits oxidized LDL-mediated upregulation of monocyte chemoattractant protein-1 and monocyte adhesion to human coronary artery endothelial cells. *Circulation*. 101:2889–2895. <https://doi.org/10.1161/01.CIR.101.25.2889>
- Li, D., L. Liu, H. Chen, T. Sawamura, S. Ranganathan, and J.L. Mehta. 2003. LOX-1 mediates oxidized low-density lipoprotein-induced expression of matrix metalloproteinases in human coronary artery endothelial cells. *Circulation*. 107:612–617. <https://doi.org/10.1161/01.CIR.0000047276.52039.FB>
- Lichtenthaler, S.F., C. Haass, and H. Steiner. 2011. Regulated intramembrane proteolysis—lessons from amyloid precursor protein processing. *J. Neurochem.* 117:779–796. <https://doi.org/10.1111/j.1471-4159.2011.07248.x>
- Lu, H., D.A. Howatt, A. Balakrishnan, M.J. Graham, A.E. Mullick, and A. Daugherty. 2016. Hypercholesterolemia Induced by a PCSK9 Gain-of-Function Mutation Augments Angiotensin II-Induced Abdominal Aortic Aneurysms in C57BL/6 Mice—Brief Report. *Arterioscler. Thromb. Vasc. Biol.* 36:1753–1757. <https://doi.org/10.1161/ATVBAHA.116.307613>
- Lu, J., X. Wang, W. Wang, H. Muniyappa, C. Hu, S. Mitra, B. Long, K. Das, and J.L. Mehta. 2012. LOX-1 abrogation reduces cardiac hypertrophy and collagen accumulation following chronic ischemia in the mouse. *Gene Ther.* 19:522–531. <https://doi.org/10.1038/gt.2011.133>
- Lutz, M.B., N. Kukutsch, A.L. Ogilvie, S. Rössner, F. Koch, N. Romani, and G. Schuler. 1999. An advanced culture method for generating large quantities of highly pure dendritic cells from mouse bone marrow. *J. Immunol. Methods*. 223:77–92. [https://doi.org/10.1016/S0022-1759\(98\)00204-X](https://doi.org/10.1016/S0022-1759(98)00204-X)

- Matsunaga, S., Q. Xie, M. Kumano, S. Niimi, K. Sekizawa, Y. Sakakibara, S. Komba, and S. Machida. 2007. Lectin-like oxidized low-density lipoprotein receptor (LOX-1) functions as an oligomer and oligomerization is dependent on receptor density. *Exp. Cell Res.* 313:1203–1214. <https://doi.org/10.1016/j.yexcr.2007.01.007>
- Matsunaga, T., S. Hokari, I. Koyama, T. Harada, and T. Komoda. 2003. NF-kappa B activation in endothelial cells treated with oxidized high-density lipoprotein. *Biochem. Biophys. Res. Commun.* 303:313–319. [https://doi.org/10.1016/S0006-291X\(03\)00308-5](https://doi.org/10.1016/S0006-291X(03)00308-5)
- Mattaliano, M.D., C. Huard, W. Cao, A.A. Hill, W. Zhong, R.V. Martinez, D.C. Harnish, J.E. Paulsen, and H.H. Shih. 2009. LOX-1-dependent transcriptional regulation in response to oxidized LDL treatment of human aortic endothelial cells. *Am. J. Physiol. Cell Physiol.* 296:C1329–C1337. <https://doi.org/10.1152/ajpcell.00513.2008>
- Mattaliano, M.D., J. Wooters, H.H. Shih, and J.E. Paulsen. 2010. ROCK2 associates with lectin-like oxidized LDL receptor-1 and mediates oxidized LDL-induced IL-8 production. *Am. J. Physiol. Cell Physiol.* 298:C1180–C1187. <https://doi.org/10.1152/ajpcell.00483.2009>
- Mehta, J.L., N. Sanada, C.P. Hu, J. Chen, A. Dandapat, F. Sugawara, H. Satoh, K. Inoue, Y. Kawase, K. Jishage, et al. 2007. Deletion of LOX-1 reduces atherosclerosis in LDLR knockout mice fed high cholesterol diet. *Circ. Res.* 100:1634–1642. <https://doi.org/10.1161/CIRCRESAHA.107.149724>
- Mentrup, T., R. Häslar, R. Fluhrer, P. Saftig, and B. Schröder. 2015. A Cell-Based Assay Reveals Nuclear Translocation of Intracellular Domains Released by SPPL Proteases. *Traffic*. 16:871–892. <https://doi.org/10.1111/tra.12287>
- Mitsuoka, H., N. Kume, K. Hayashida, A. Inui-Hayashida, Y. Aramaki, M. Toyohara, T. Jinai, E. Nishi, and T. Kita. 2009. Interleukin 18 stimulates release of soluble lectin-like oxidized LDL receptor-1 (sLOX-1). *Atherosclerosis*. 202:176–182. <https://doi.org/10.1016/j.atherosclerosis.2008.04.002>
- Murase, T., N. Kume, H. Kataoka, M. Minami, T. Sawamura, T. Masaki, and T. Kita. 2000. Identification of soluble forms of lectin-like oxidized LDL receptor-1. *Arterioscler. Thromb. Vasc. Biol.* 20:715–720. <https://doi.org/10.1161/01.ATV.20.3.715>
- Murphy, J.E., R.S. Vohra, S. Dunn, Z.G. Holloway, A.P. Monaco, S. Homer-Vanniasinkam, J.H. Walker, and S. Ponnambalam. 2008. Oxidized LDL internalisation by the LOX-1 scavenger receptor is dependent on a novel cytoplasmic motif and is regulated by dynamin-2. *J. Cell Sci.* 121:2136–2147. <https://doi.org/10.1242/jcs.020917>
- Nicolaou, A., Z. Zhao, B.H. Northoff, K. Sass, A. Herbst, A. Kohlmaier, A. Chalaris, C. Wolfrum, C. Weber, S. Steffens, et al. 2017. Adam17 Deficiency Promotes Atherosclerosis by Enhanced TNFR2 Signaling in Mice. *Arterioscler. Thromb. Vasc. Biol.* 37:247–257. <https://doi.org/10.1161/ATVBAHA.116.308682>
- Pirillo, A., and A.L. Catapano. 2013. Soluble lectin-like oxidized low density lipoprotein receptor-1 as a biochemical marker for atherosclerosis-related diseases. *Dis. Markers*. 35:413–418. <https://doi.org/10.1155/2013/716325>
- Plato, A., J.A. Willment, and G.D. Brown. 2013. C-type lectin-like receptors of the lectin-1 cluster: ligands and signaling pathways. *Int. Rev. Immunol.* 32:134–156. <https://doi.org/10.3109/08830185.2013.777065>
- Radons, J., V. Faber, H. Buhrmester, W. Völker, V. Horejsi, and A. Hasilik. 1992. Stimulation of the biosynthesis of lactosamine repeats in glycoproteins in differentiating U937 cells and its suppression in the presence of NH4Cl. *Eur. J. Cell Biol.* 57:184–192.
- Raines, E.W. 2004. PDGF and cardiovascular disease. *Cytokine Growth Factor Rev.* 15:237–254. <https://doi.org/10.1016/j.cytogfr.2004.03.004>
- Riethmueller, S., J.C. Ehlers, J. Lokau, S. Düsterhöft, K. Knittler, G. Dombrowsky, J. Grötzinger, B. Rabe, S. Rose-John, and C. Garbers. 2016. Cleavage Site Localization Differentially Controls Interleukin-6 Receptor Proteolysis by ADAM10 and ADAM17. *Sci. Rep.* 6:25550. <https://doi.org/10.1038/srep25550>
- Rogers, M.A., N. Maldonado, J.D. Hutcheson, C. Goettsch, S. Goto, I. Yamada, T. Faits, H. Sesaki, M. Aikawa, and E. Aikawa. 2017. Dynamin-Related Protein 1 Inhibition Attenuates Cardiovascular Calcification in the Presence of Oxidative Stress. *Circ. Res.* 121:220–233. <https://doi.org/10.1161/CIRCRESAHA.116.310293>
- Sawamura, T., N. Kume, T. Aoyama, H. Moriwaki, H. Hoshikawa, Y. Aiba, T. Tanaka, S. Miwa, Y. Katsura, T. Kita, and T. Masaki. 1997. An endothelial receptor for oxidized low-density lipoprotein. *Nature*. 386:73–77. <https://doi.org/10.1038/386073a0>
- Schneppenheim, J., R. Dressel, S. Hüttl, R. Lüllmann-Rauch, M. Engelke, K. Dittmann, J. Wienands, E.L. Eskelinen, I. Hermans-Borgmeyer, R. Fluhrer, et al. 2013. The intramembrane protease SPPL2a promotes B cell development and controls endosomal traffic by cleavage of the invariant chain. *J. Exp. Med.* 210:41–58. <https://doi.org/10.1084/jem.20121069>
- Schneppenheim, J., S. Hüttl, A. Kruchen, R. Fluhrer, I. Müller, P. Saftig, R. Schneppenheim, C.L. Martin, and B. Schröder. 2014a. Signal-peptide-peptidase-like 2a is required for CD74 intramembrane proteolysis in human B cells. *Biochem. Biophys. Res. Commun.* 451:48–53. <https://doi.org/10.1016/j.bbrc.2014.07.051>
- Schneppenheim, J., S. Hüttl, T. Mentrup, R. Lüllmann-Rauch, M. Rothaug, M. Engelke, K. Dittmann, R. Dressel, M. Araki, K. Araki, et al. 2014b. The intramembrane proteases signal Peptide peptidase-like 2a and 2b have distinct functions in vivo. *Mol. Cell. Biol.* 34:1398–1411. <https://doi.org/10.1128/MCB.00038-14>
- Schröder, B., C. Wrocklage, A. Hasilik, and P. Saftig. 2010. Molecular characterisation of ‘transmembrane protein 192’ (TMEM192), a novel protein of the lysosomal membrane. *Biol. Chem.* 391:695–704. <https://doi.org/10.1515/bc.2010.062>
- Schuermann, M. 1990. An expression vector system for stable expression of oncogenes. *Nucleic Acids Res.* 18:4945–4946. <https://doi.org/10.1093/nar/18.16.4945>
- Schwartz, M. 2004. Rho signalling at a glance. *J. Cell Sci.* 117:5457–5458. <https://doi.org/10.1242/jcs.01582>
- Shevchenko, A., H. Tomas, J. Havlis, J.V. Olsen, and M. Mann. 2006. In-gel digestion for mass spectrometric characterization of proteins and proteomes. *Nat. Protoc.* 1:2856–2860. <https://doi.org/10.1038/nprot.2006.468>
- Singer, C.A., B. Lontay, H. Unruh, A.J. Halayko, and W.T. Gerthoffer. 2011. Src mediates cytokine-stimulated gene expression in airway myocytes through ERK MAPK. *Cell Commun. Signal.* 9:14. <https://doi.org/10.1186/1478-811X-9-14>
- Steinberg, D., S. Parthasarathy, T.E. Carew, J.C. Khoo, and J.L. Witztum. 1989. Beyond cholesterol. Modifications of low-density lipoprotein that increase its atherogenicity. *N. Engl. J. Med.* 320:915–924.
- Thakkar, S., X. Wang, M. Khaidakov, Y. Dai, K. Gokulan, J.L. Mehta, and K.I. Varughese. 2015. Structure-based Design Targeted at LOX-1, a Receptor for Oxidized Low-Density Lipoprotein. *Sci. Rep.* 5:16740. <https://doi.org/10.1038/srep16740>
- Theodorou, K., E.P.C. van der Vorst, M.J. Gijbels, I.M.J. Wolfs, M. Jeurissen, T. L. Theelen, J.C. Sluimer, E. Wijnands, J.P. Cleutjens, Y. Li, et al. 2017. Whole body and hematopoietic ADAM8 deficiency does not influence advanced atherosclerotic lesion development, despite its association with human plaque progression. *Sci. Rep.* 7:11670. <https://doi.org/10.1038/s41598-017-10549-x>
- Treitz, C., L. Cassidy, A. Höckendorf, M. Leippe, and A. Tholey. 2015. Quantitative proteome analysis of Caenorhabditis elegans upon exposure to nematocidal Bacillus thuringiensis. *J. Proteomics*. 113:337–350. <https://doi.org/10.1016/j.jpropt.2014.09.027>
- van der Vorst, E.P., M. Jeurissen, I.M. Wolfs, A. Keijbeck, K. Theodorou, E. Wijnands, L. Schurgers, S. Weber, M.J. Gijbels, A.A. Hamers, et al. 2015. Myeloid A disintegrin and metalloproteinase domain 10 deficiency modulates atherosclerotic plaque composition by shifting the balance from inflammation toward fibrosis. *Am. J. Pathol.* 185:1145–1155. <https://doi.org/10.1016/j.ajpath.2014.11.028>
- Voss, M., B. Schröder, and R. Fluhrer. 2013. Mechanism, specificity, and physiology of signal peptide peptidase (SPP) and SPP-like proteases. *Biochim. Biophys. Acta*. 1828:2828–2839. <https://doi.org/10.1016/j.bbame.2013.03.033>
- Wang, X., M. Khaidakov, Z. Ding, S. Mitra, J. Lu, Y. Dai, and J.L. Mehta. 2012. Lectin-like oxidized low-density lipoprotein receptor-1 (LOX-1) and cardiac fibroblast growth. *Hypertension*. 60:1437–1442. <https://doi.org/10.1161/HYPERTENSIONAHA.112.200659>
- White, S.J., G.B. Sala-Newby, and A.C. Newby. 2011. Overexpression of scavenger receptor LOX-1 in endothelial cells promotes atherosclerosis in the ApoE(-/-) mouse model. *Cardiovasc. Pathol.* 20:369–373. <https://doi.org/10.1016/j.carpath.2010.08.007>
- Wolpe, S.D., B. Sherry, D. Juers, G. Davatilis, R.W. Yurt, and A. Cerami. 1989. Identification and characterization of macrophage inflammatory protein 2. *Proc. Natl. Acad. Sci. USA*. 86:612–616. <https://doi.org/10.1073/pnas.86.2.612>
- Wunderlich, P., K. Glebov, N. Kemmerling, N.T. Tien, H. Neumann, and J. Walter. 2013. Sequential proteolytic processing of the triggering receptor expressed on myeloid cells-2 (TREM2) protein by ectodomain shedding and γ -secretase-dependent intramembranous cleavage. *J. Biol. Chem.* 288:33027–33036. <https://doi.org/10.1074/jbc.M113.517540>

- Xu, S., S. Ogura, J. Chen, P.J. Little, J. Moss, and P. Liu. 2013. LOX-1 in atherosclerosis: biological functions and pharmacological modifiers. *Cell. Mol. Life Sci.* 70:2859–2872. <https://doi.org/10.1007/s00018-012-1194-z>
- Yang, T.C., P.Y. Chang, T.L. Kuo, and S.C. Lu. 2017. Electronegative L5-LDL induces the production of G-CSF and GM-CSF in human macrophages through LOX-1 involving NF- κ B and ERK2 activation. *Atherosclerosis*. 267:1–9. <https://doi.org/10.1016/j.atherosclerosis.2017.10.016>
- Zhao, X.Q., M.W. Zhang, F. Wang, Y.X. Zhao, J.J. Li, X.P. Wang, P.L. Bu, J.M. Yang, X.L. Liu, M.X. Zhang, et al. 2011. CRP enhances soluble LOX-1 release from macrophages by activating TNF- α converting enzyme. *J. Lipid Res.* 52:923–933. <https://doi.org/10.1194/jlr.M015156>
- Zhao, Y., M. Lv, H. Lin, Y. Hong, F. Yang, Y. Sun, Y. Guo, Y. Cui, S. Li, and Y. Gao. 2012. ROCK1 induces ERK nuclear translocation in PDGF-BB-stimulated migration of rat vascular smooth muscle cells. *IUBMB Life*. 64:194–202. <https://doi.org/10.1002/iub.598>
- Zhu, H., M. Xia, M. Hou, Z. Tang, Y. Li, J. Ma, and W. Ling. 2005. Ox-LDL plays dual effect in modulating expression of inflammatory molecules through LOX-1 pathway in human umbilical vein endothelial cells. *Front. Biosci.* 10:2585–2594. <https://doi.org/10.2741/1722>
- Zhu, S.N., M. Chen, J. Jongstra-Bilen, and M.I. Cybulsky. 2009. GM-CSF regulates intimal cell proliferation in nascent atherosclerotic lesions. *J. Exp. Med.* 206:2141–2149. <https://doi.org/10.1084/jem.20090866>